

Star-Planet Interactions: Observational Techniques and Methods

P. Figueira^{*1,2}, H. Korhonen³, A. Buccino^{4,5}, P. Chaturvedi⁶, R. Fares⁷,
A. García-Muñoz⁸, B. Montet⁹, L. Peña-Moñino², M. Pérez-Torres², D. Revilla², and
A. Valio¹⁰

¹Observatoire Astronomique de l'Université de Genève, Chemin Pegasi 51b, 1290 Versoix, Switzerland

²Instituto de Astrofísica de Andalucía-CSIC, Glorieta de la Astronomía s/n, 18008 Granada, Spain

³Max-Planck-Institut für Astronomie, Königstuhl 17, D-69117 Heidelberg, Germany

⁴Departamento de Física, FCEyN Universidad de Buenos Aires, Buenos Aires, Argentina

⁵Instituto de Astronomía y Física del Espacio (UBA-CONICET), Buenos Aires, Argentina

⁶Department of Astronomy and Astrophysics, Tata Institute of Fundamental Research, Mumbai, India

⁷Department of Physics, College of Science, United Arab Emirates University, P.O. Box 15551, Al Ain, UAE

⁸Université Paris-Saclay, Université Paris Cité, CEA, CNRS, AIM, 91191, Gif-sur-Yvette, France

⁹School of Physics, University of New South Wales, Kensington 2052, Australia

¹⁰Centro de Rádio Astronomia e Astrofísica Mackenzie (CRAAM), Universidade Presbiteriana Mackenzie, São Paulo, Brazil

Abstract

This chapter summarizes the techniques and methods used to study star-planet interaction (SPI) from the observational point of view. SPI can produce a wide range of observational signatures, from localized stellar activity enhancements to changes in planetary atmospheric escape and transmission spectra. This chapter reviews the main observational techniques used to detect and characterize SPI, emphasizing the methodological challenges involved in separating planet-induced signals from intrinsic stellar variability. We discuss radial-velocity diagnostics, including cross-correlation, template matching, line-by-line methods, and activity indicators, highlighting their sensitivity to line-profile distortions and chromatic variability. We then review precision photometry as a tool to search for orbit-locked variability, flare modulation, and active-region occultations during planetary transits, with particular attention to detrending, correlated-noise modeling, Gaussian processes, and statistical validation. Chromospheric diagnostics, including Ca II, H α , He I, and Na II lines, are presented as tracers of magnetic variability at different atmospheric heights and as potential probes of intermittent SPI signatures. We also discuss transmission spectroscopy as a complementary approach, since planetary atmospheric tracers such as H I Ly α , Balmer lines, C II, and He I can encode information about the stellar high-energy environment, stellar wind, and magnetic coupling. In addition, radio observations provide a promising avenue to probe magnetic SPI directly through coherent emission mechanisms, offering unique constraints on planetary magnetic fields and star-planet coupling. Finally, we examine time-series analysis techniques commonly employed in SPI searches, including generalized Lomb-Scargle periodograms, rolling periodograms, harmonic analyses, and bootstrap-based significance estimation, with emphasis on the identification of transient and orbit-related signals in unevenly sampled datasets. Together, these methods show that robust SPI identification requires coherent evidence across timescales, diagnostics, and atmospheric layers, rather than a single periodic signal.¹

The authors have no relevant financial or non-financial interests to disclose, and no competing interests to declare that are relevant to the content of this article.

The authors have no conflicts of interest to declare.

*corresponding author; pedro.figueira@iaa.es

¹The instrumentation that employs these methods is presented in the companion chapter Korhonen et al. (2026).

Introduction

The methods used to study SPI are as diverse as the range of possible star–planet interaction signatures. Moreover, the difficulty of establishing a “smoking gun” signature—one that unambiguously confirms the interaction—has led to a proliferation of detection and characterization efforts. Here, we outline the various methods employed in the study of star–planet interactions (SPI), either by explaining their fundamental principles in the context of SPI or by introducing them in general terms and subsequently discussing their specific applications to SPI.

Radial Velocities

Precise radial velocity (RV) measurements have been fundamental to our understanding of stellar properties in the solar neighbourhood (Duquennoy and Mayor, 1991). Following the detection of the first planet orbiting a Sun-like star by Mayor and Queloz (1995), this technique came under close scrutiny. Because of its sensitivity to variations in the positions and shapes of photospheric lines, it also traces stellar activity and, by extension, activity induced by the presence of a planet.

We group the different RV calculation methods according to their underlying assumptions and methodologies, and complement these by a brief description of associated activity indicators. We conclude the section by discussing how these RV signatures can be identified in time series data in practice.

Fourier domain methods and spectral information content

A foundational approach to RV calculation was outlined by Chelli (2000), who considered the case of an observed spectrum that differs from a reference spectrum only through an RV shift and the presence of photon noise. The author provided a framework for an optimally weighted RV calculation in Fourier space. In practice, the reference spectrum can be constructed by co-adding a large number of spectra, and working in Fourier space allows the filtering of both high and low frequencies, corresponding to photon noise and continuum variations, respectively. For an efficient application of this framework to A–F main-sequence stars, the reader is referred to Galland et al. (2005).

The optimal weighting principles proposed by Chelli (2000) define thus a best-case scenario for RV calculation, and motivated the study of spectral information content by Bouchy et al. (2001). These authors provided a methodology, this time in the wavelength domain, both to calculate the RV and to estimate the RV precision achievable for a given spectrum in the presence of photon noise alone. This method has since become invaluable for estimating the precision achievable in the high-S/N regime, as is often reached in RV surveys of bright stars. Moreover, it provides an important physical insight: the RV information content of a spectral line is proportional to the local slope of the flux and is therefore concentrated in the *wings* of the line.

While this method was a cornerstone in the development of precise RV measurements, it assumes that the spectrum remains unchanged apart from an RV shift and noise. As such, it cannot identify signatures that depend on wavelength or spectral lines, nor those that alter the global properties of the spectrum. Its usage in SPI studies is therefore limited.

The cross-correlation function

The cross-correlation function (CCF) method, used in the detection of the first extrasolar planets around main-sequence stars, makes fewer assumptions than Fourier-domain approaches. In a nutshell, an observed spectrum is cross-correlated with a “mask”, i.e. a template containing the rest wavelengths of selected spectral lines. The resulting cross-correlation function can be interpreted as an average line profile in velocity space, from which RVs are typically measured with a simple Gaussian fitting. The method is presented in detail by Baranne et al. (1996). The work of Pepe et al. (2002) further developed this approach by introducing weighted lines, i.e., assigning each line a weight proportional

to its information content. In early implementations, these weights were simply proportional to the line contrast; in modern pipelines, they are computed from detailed line properties and instrumental characteristics (e.g. [Figueira, 2018](#)).

When considering how to optimally combine cross-correlation functions, it is particularly insightful to revisit [Zucker \(2003\)](#), who provided a statistically rigorous framework for their combination. However, this method draws its strength and rigour by remaining fundamentally tied to the assumption that the observed spectrum differs from the template primarily through a Doppler shift. This undermines its diagnostic power for SPI signatures that manifest as line-dependent or chromatic spectral distortions, a limitation common to all similar approaches.

Within the context of CCF analysis, [Collier Cameron et al. \(2021\)](#) represents a significant step forward. This work introduced a wavelength-domain, data-driven method to separate genuine planetary reflex Doppler shifts from apparent RV variations induced by stellar variability. The method exploits the fact that the autocorrelation of the CCF is invariant to RV shifts, whereas stellar activity induces distortions in line profiles. It then uses principal component analysis of the CCF autocorrelation to isolate these shape-driven modes. Because SPI-related signals may manifest as line-profile or wavelength-dependent variability rather than as pure center-of-mass motion, methods such as that of [Collier Cameron et al. \(2021\)](#) are particularly valuable for distinguishing physically distinct sources of apparent RV variability. This method, named SCALPELS, has been successfully applied to very high-S/N solar spectra and holds significant promise for studying SPI in bright stars.

The template matching approach

As exoplanet searches began to target M dwarfs, it became apparent that applying the CCF method to these stars was considerably more challenging. Constructing line masks was difficult, as theoretical spectra suffered from incomplete line lists and the numerous but shallow lines of M dwarfs remained poorly defined even in observed spectra with high S/N. In addition, their spectra are strongly affected by pseudo-continuum absorption, and the stars themselves are relatively faint for most spectrographs. These three difficulties worked together quite well, much to the frustration of observers.

[Kürster et al. \(2003\)](#) proposed a different approach: calculating RVs through a χ^2 - match between the observed spectrum and a shifted template spectrum. High-S/N templates could be constructed by co-adding many observed spectra, and the minimum of $\chi^2(\text{RV})$ yielded the stellar RV. This allowed to reach a precision of 2.7 m/s on Barnard’s star using UVES, an impressive result for the time. It laid part of the methodological foundation for the landmark detection of Proxima b by [Anglada-Escudé et al. \(2016\)](#) using HARPS spectra. In that work, the authors revealed the presence of a short-period planet around our nearest stellar neighbour, showcasing the power of template matching.

Today, several template-matching methods exist and are routinely used. [SERVAL \(Zechmeister et al., 2018\)](#), widely used with CARMENES (e.g. [Trifonov et al., 2018](#)), is probably the best known. [S-BART \(Silva et al., 2022\)](#) provides a more modern implementation with somewhat different technical choices. It is worth noting that, to date, one of the most precise long-term RV baselines has been obtained with S-BART on ESPRESSO data: 40 cm/s over 3.5 yr on τ Ceti ([Figueira et al., 2025](#)). The modest gain in precision for this K dwarf relative to the CCF method may result from a better leveraging of the spectral information content, including the continuum, or from a greater robustness to flux systematics, although it is impossible to be sure and the method is still under active investigation. [Silva et al. \(2025\)](#) recently highlighted that template-matching methods can be affected by intra-night RV slopes under specific conditions, and caution is therefore warranted.

Because template matching assumes a constant reference spectrum, it is intrinsically ill-suited to SPI signatures that manifest through changes in the properties of individual spectral lines. Moreover, recent developments have shown that, despite its remarkable precision, the method still involves subtle technical choices with an impact that is not yet fully understood.

Line-by-line methods

It has long been known that, in the Sun, different photospheric spectral lines exhibit varying sensitivity to the level of stellar activity ([Gray, 2005b](#)). This motivated several studies aimed at measuring the RVs of individual spectral lines (e.g. [Dumusque, 2018](#); [Cretignier et al., 2020](#)). These studies generally rely on a large number of high-S/N spectra, acquired with instruments with highly stabilized instrumental

profiles, such as HARPS, to measure the RV variations of individual lines and assess their sensitivity to stellar activity.

Among the different implementations of the line-by-line approach, [Artigau et al. \(2022\)](#) provided a particularly clear formalization of the method, emphasizing the advantages of treating individual spectral lines as independent RV estimators. Although primarily motivated by the treatment of outlying spectral information, this methodology applies directly to stellar activity and SPI. More recently, [Martinez et al. \(2026\)](#) explored a similar strategy, reinforcing the idea that line-resolved measurements can provide a more physically informative view of stellar and planetary signals.

By avoiding the compression of the full spectrum into a single average profile, these methods retain information that may otherwise be lost in global RV estimators. This is particularly relevant for SPI studies, in which the signal may affect only specific lines or classes of lines rather than the spectrum as a whole.

Radial Velocity Activity Indicators

The detection of exoplanets via RV is an indirect method, and from the earliest discoveries there has been concern about false-positive signals. This led to the development of activity indicators derived from the same spectra used to measure RVs. The most widely used of these is the bisector inverse span (BIS), popularized in the context of exoplanet detection by [Queloz et al. \(2001\)](#). In this approach, the bisector of the CCF is measured in a manner analogous to that used for individual spectral lines in stellar physics (e.g. [Gray, 2005a](#)).

Another important indicator is the full width at half maximum (FWHM) of the lines, often measured on the CCF. When derived from spectra obtained through a spectrograph with stabilized instrumental profile, variations in the FWHM primarily trace changes in the widths of spectral lines, and thus stellar activity. This has been used effectively to identify and model rotational modulation, for example in the ESPRESSO campaign of [Faria et al. \(2022\)](#). The line contrast can also serve as an activity proxy, alongside a broader set of indicators (see, e.g. [Figueira et al., 2013](#); [Simola et al., 2019](#); [Barnes et al., 2024](#)). However, these indicators often exhibit different sensitivities and correlations with RVs in active stars, as shown, for instance, by [Lafarga et al. \(2020\)](#), making their interpretation non-trivial.

In addition to line-shape diagnostics, wavelength-dependent indicators have been developed to probe activity-induced RV variations. Since the reflex motion induced by a planet is, to first order, achromatic, measurements of RVs as a function of wavelength have long been used to identify signals arising from stellar activity (e.g. [Huélamo et al., 2008](#)). In this context, several wavelength-dependent diagnostics have been developed to flag false positives, including the chromatic index (CRX) implemented in *SERVAL* ([Zechmeister et al., 2018](#)) and the *dTemp* indicator introduced by [Artigau et al. \(2022\)](#).

While these indicators can be straightforwardly derived from spectral lines or CCFs, they inherit the limitations associated with compressing the spectral information into a small number of scalar quantities, and may therefore miss line-dependent or chromatic signatures relevant to SPI.

Precise RV measurements and their associated diagnostics provide a rich framework for studying SPI. Methods based on global spectral compression, such as Fourier-domain approaches, CCFs, and template matching, have enabled the extraordinary precision required for exoplanet detection, but they remain fundamentally optimized for signals that are affected by pure Doppler shifts. In contrast, SPI signatures are likely to manifest through subtle line-dependent, chromatic, or profile-shape variations that violate these assumptions. The more flexible and information-preserving approaches, including line-by-line analyses and data-driven decompositions of spectral variability draw us significantly closer to the objective of characterizing SPI. As a whole, the developments illustrate a broader transition in high-precision spectroscopy: from measuring a single scalar RV toward exploiting the full physical information stored in a stellar spectra.

Precision Photometry from stellar surveys

Precision time-series photometry provides a powerful avenue for studying SPI by enabling continuous monitoring of stellar brightness over timescales short enough to resolve stellar granulation signatures to those long enough to analyse stellar magnetic activity cycles. Unlike spectroscopic techniques, which probe localised diagnostics such as line cores or chromospheric emission, photometry measures the integrated response of the stellar photosphere. It is therefore sensitive to stellar activity across spatial scales, including starspots, faculae, flares, and transient occultations of active regions by orbiting planets (see, for example [Huber, 2025](#), and references therein).

From a methodological perspective, the primary challenge in photometric SPI studies is often not the detection of variability, but the robust separation of small, potentially planet-linked signals from other intrinsic stellar variability and instrumental systematics. Consequently, the effectiveness of photometry for SPI rests largely on advances in time-series analysis, correlated-noise modelling, and statistical inference (e.g. [Cubillos et al., 2017](#)).

Often, when we consider SPI, we are interested in photometric signals that occur with the same periodicity as that of an orbiting planet. To separate an SPI signal from these other factors, we then consider a useful conceptual decomposition of a photometric time series as

$$y(t) = m_{\star}(t) + m_{\text{orb}}(t) + m_{\text{tr}}(t) + s(t) + \epsilon(t), \quad (1)$$

where $m_{\star}(t)$ represents intrinsic stellar variability, $m_{\text{orb}}(t)$ any stellar component that occurs with the same period as the planetary orbit, $m_{\text{tr}}(t)$ geometric apparent signals such as planet transits, $s(t)$ is any instrumental systematics, and $\epsilon(t)$ the residual noise. The methodological goal is to determine whether $m_{\text{orb}}(t)$ is required by the data once realistic models of $m_{\star}(t)$ and instrumental effects are taken into account (for more details, consider [Boisse et al., 2011](#); [McQuillan et al., 2012](#))

Separating Astrophysics from Instrumental Systematics

Detrending is among the most consequential steps in photometric analyses of SPI. Many instrumental systematics, whether observations are collected from the ground or from space, occupy a similar frequency space as SPI signatures. The choice of how detrending is accomplished, or whether it is done at all, is a scientific choice that directly affects sensitivity, false-positive rates, and interpretability. Effective detrending aims not to remove variability, but to separate components in a manner that preserves astrophysical signals while suppressing non-astrophysical ones, and effectively preserves information about the uncertainty inherent in the choices of detrending algorithm applied (e.g. [Morello, 2015](#); [Hippke et al., 2019](#); [Taaki et al., 2020](#)).

Two opposing failure modes dominate SPI analyses. *Over-detrending* occurs when the detrending model is overly flexible and absorbs genuine astrophysical variability. This risk is highest when basis vectors or smoothing functions span timescales comparable to the stellar rotation or planetary orbital period, or when detrending is performed independently on short data segments, thereby destroying long-term phase coherence. Over-detrending biases results toward null detections and systematically underestimates signal amplitudes.

Under-detrending, by contrast, leaves residual systematics that can masquerade as astrophysical signals. Low-frequency instrumental trends, cadence changes, and data gaps can imprint spurious periodicities or harmonics that align coincidentally with orbital phase. Under-detrending inflates false-positive rates and can lead to apparently coherent SPI signatures that disappear under alternative preprocessing choices. Any result must demonstrate that it is not sensitive to the choice of detrending approach applied.

Families of Detrending Approaches

Several methodological families are commonly employed to separate astrophysics from systematics.

Parametric and basis-vector detrending. Here, systematics are modeled as a linear combination of basis vectors,

$$s(t) = \sum_k c_k B_k(t), \quad (2)$$

where $B_k(t)$ is inferred from low-rank trends derived from ensembles of stars or regressors tied to known instrumental states. These may be found through an approach similar to principal component analysis, in which a set of orthogonal eigenvectors are calculated which parameterise the information shared across the entire ensemble. This approach is efficient and interpretable. However, it requires the basis vectors to not contain information with similar behavior to the astrophysical signals produced by the star. This was the primary approach of the “pre-search data conditioning” method of the *Kepler* data analysis pipeline, which aimed to remove signals on both short and long timescales (Smith et al., 2012; Stumpe et al., 2012, 2014)

Filtering and smoothing. High-pass filters, running medians, or spline fits are often used to remove low-frequency trends. One of the most common is a Savitzky-Golay filter (Savitzky and Golay, 1964), which is a common “flattening” function in transiting planet analyses in which a low-degree polynomial is fit to a local window around each individual data point, and the calculated value of that polynomial at each point applied as the predicted model. While simple, such filters impose an implicit transfer function on the data. This approach also assumes the noise properties of the data are unchanged throughout the window of observations, as each data point is given equal weight. The underlying data is also assumed to be characteristic of this smooth polynomial; any sharp features such as transits or stellar flares will bias this result. In SPI applications, filtering must be chosen so that its characteristic cutoff lies well away from both the stellar rotation and planetary orbital periods; otherwise, genuine phase-coherent signals may be attenuated or distorted (e.g. Lanza, 2008).

Joint modeling of systematics and astrophysics. A more robust approach is to model systematics and astrophysical variability simultaneously, allowing uncertainty in their separation to propagate naturally into the final inference. Foreman-Mackey et al. (2017) use 150 basis vectors rather than the standard 4-16 but simultaneously fit these with a transit model, reducing the risk of overfitting.

This joint formulation allows correlations between instrumental effects and stellar variability to be handled self-consistently, reducing biases that can arise when detrending and astrophysical modeling are performed sequentially. This approach is often implemented by combining low-dimensional parametric models or basis-vector representations for $s(t)$ with flexible stochastic models for $m_\star(t)$, such as Gaussian Processes, and explicit phase-locked components for $m_{\text{orb}}(t)$. A key advantage of joint modeling is that uncertainty in the decomposition of variability is propagated into the posterior distributions of the SPI parameters, rather than being fixed at an earlier preprocessing stage. The principal drawbacks are increased computational cost, sensitivity to prior assumptions, and the need for careful model comparison to avoid overfitting, particularly when the systematics and astrophysical signals share similar characteristic timescales. In practice, joint modeling is most useful when instrumental systematics and stellar variability operate on overlapping timescales, when the SPI signal of interest is expected to be low amplitude, or when the scientific conclusions depend sensitively on propagating detrending uncertainty into the final inference.

Modeling Stellar Variability as Correlated Noise

Stellar photometric variability is neither white nor stationary: signals arising from starspots and faculae evolve in amplitude and phase as active regions grow, decay, and migrate across the stellar surface. For SPI studies, this variability is typically a nuisance signal that must be modeled and marginalized over to test for smaller, planet-linked effects. Gaussian Process (GP) regression has therefore become a widely used and practical tool for modeling stellar variability in photometric time series (Aigrain and Foreman-Mackey, 2023, and references therein).

A GP can be understood as a flexible way of describing what stellar variability usually looks like without committing to a specific physical spot model. Instead of fitting individual spots, the GP builds models consistent with the expected covariance of the light curve: points close together in time are more similar than distant ones, and variability often repeats approximately on the stellar rotation period while evolving over longer timescales.

A commonly used kernel for rotational modulation is the quasi-periodic form

$$k(t, t') = A^2 \exp \left[-\frac{(t - t')^2}{2\lambda^2} - \Gamma^2 \sin^2 \left(\frac{\pi(t - t')}{P_{\text{rot}}} \right) \right], \quad (3)$$

where P_{rot} represents the stellar rotation period, λ the typical lifetime of active regions, and A the overall variability amplitude. In practice, this kernel captures the intuitive picture of a light curve that is approximately periodic but slowly changing from one rotation to the next (Angus et al., 2018).

In SPI analyses, the GP is rarely the quantity of interest itself. Rather, it serves as a flexible model for stellar variability that allows other components of the light curve to be tested more robustly. Potential SPI signatures are introduced as explicit orbital-phase terms, such as a sinusoid or low-order Fourier series at the planetary orbital period, and the question becomes whether the data prefer a model that includes both stellar variability and a phase-locked component over one that includes stellar variability alone.

A key strength of the GP approach is that it naturally accounts for correlated noise and propagates uncertainty in the stellar variability model into the inferred properties of any SPI signal. However, GPs are limited by the assumptions of the noise properties of the kernel itself, as well as the priors applied. In particular, if the GP contains periodic terms which are close in frequency to the planetary orbital period or its harmonics, a GP can absorb genuine phase-locked signals (e.g. Foreman-Mackey et al., 2017).

For this reason, GP-based analyses in SPI studies should be accompanied by explicit null tests and injection-recovery experiments to verify that orbit-locked signals of interest are not affected by the modeling procedure.

Flare Detection and Orbital-Phase Statistics

Stellar flares appear in photometric time series as impulsive, asymmetric brightenings with a rapid rise and more gradual decay. In the context of SPI studies, flares are of particular interest because magnetic interactions between a star and a close-in planet have been proposed as a possible trigger or modulator of flare activity (Ilin et al., 2025). To test this, we then must be able to reliably identify flares in survey photometry and test whether their occurrence shows any preference for particular planetary orbital phases².

Flare detection typically begins with the removal of low-frequency variability associated with stellar rotation and instrumental trends. This step is intended to flatten the local baseline without suppressing impulsive events (e.g. Davenport, 2016). Candidate flares are then identified as statistically significant upward excursions above the local noise level, using a simple flare template (Notsu et al., 2013), or sometimes a machine learning approach (Vida and Roettenbacher, 2018; Feinstein et al., 2020).

Once flares are identified, each event time is converted into an orbital phase, in order to test whether flares preferentially cluster at specific orbital phases. This typically involves randomizing flare times within the observed time windows to estimate how often comparable clustering would arise by chance (e.g. Tofflemire et al., 2017; Ilin et al., 2025). The phase conversion is done relative to a reference time T_0 (for example the transit midpoint), together with either the orbital period P_{orb} or the synodic period P_{syn} .

In most datasets, flare detectability is not uniform in time. Variations in noise level, data gaps, and detrending efficiency all affect the probability of detecting a flare at a given epoch, and must be accounted for in data analyses. This is further compounded by intrinsic stellar variability, since stars with similar spot coverage can exhibit markedly different flare occurrence rates, likely reflecting differences in magnetic complexity rather than spot area alone (Araújo and Valio, 2023).

Mapping Stellar Surfaces

For transiting systems, precision photometry provides a unique opportunity to probe stellar surface structure through the analysis of starspot and facular crossings. Spots and faculae produce brightness variations on a rotational timescale (e.g. Berdyugina, 2005; Oshagh et al., 2013). When a planet occults an active region on the stellar surface, the resulting transit light curve deviates locally from the smooth profile expected for a uniform photosphere (Silva, 2003). These anomalies appear as short-duration

²See, however, the different flare signature triggered by magnetic SPI and proposed for GJ 436 by Loyd et al. (2023).

brightenings or dimmings within transits and offer spatially resolved information about stellar activity that is otherwise inaccessible in disk-integrated photometry (Morris et al., 2017).

This analysis typically begins with fitting a standard transit model to each individual transit event, with residuals inspected for statistically significant localized features. The timing, duration, and amplitude of these events is sufficient to infer their approximate position, size, and intensity along the transit chord (Silva-Valio and Lanza, 2011; Zaleski et al., 2022; Araújo and Valio, 2023).

By converting the timing of each anomaly into a position on the stellar surface, spot-crossing events can be mapped to stellar longitudes (Lanza et al., 2009; Valio et al., 2017). Repeated transits allow these active regions to be tracked over time, providing constraints on spot lifetimes, differential rotation (Silva-Valio and Lanza, 2011; Valio et al., 2017; Araújo and Valio, 2021; Zaleski et al., 2022; Valio et al., 2024), and the persistence of preferred active longitudes (Nutzman et al., 2011; Sanchis-Ojeda and Winn, 2011). When spot-crossing events recur at similar stellar longitudes over many transits, they indicate long-lived surface structures. Moreover, transit spot mapping enables the estimation of starspot magnetic fields through calibrated relations between spot flux deficit and magnetic field, yielding typical values of $\sim 2.74.6$ kG across FGK and M stars (Menezes et al., 2024). In parallel, it provides robust measurements of spot filling factors, with surface coverage ranging from a few percent up to $\sim 30\%$, revealing that the decline of stellar magnetic activity with age is primarily driven by a reduction in spot coverage rather than in field strength (Araújo et al., 2025).

For SPIs, a primary question is often whether such active regions show a systematic relationship with the planetary orbit. This may manifest as spot crossings occurring preferentially at specific orbital phases or longitudes tied to the planet’s position (Shkolnik et al., 2008a; Pagano et al., 2009).

Several limitations must be borne in mind when interpreting spot-crossing signatures. The stellar surface properties remain ambiguous when a transit is not occurring because of a loss of information as a stellar surface is projected into a 1-dimensional time series (Luger et al., 2021; Deagan and Montet, 2026). Small or low-contrast active regions may escape detection, leading to incomplete surface maps. Degeneracies between spot size, contrast, and latitude can complicate physical interpretation, particularly for grazing transits. In addition, apparent recurrence of anomalies can arise spuriously if the stellar rotation period is close to an integer multiple of the orbital period.

Statistical Validation and Sensitivity Limits

Most photometric SPI signals are subtle and require statistical validation; many studies are based on population-level inference rather than analysis of a single star. Statistical significance must be evaluated relative to realistic null models. These are rarely white noise, but rather include evolving stellar variability, correlated noise, and complicated observing window functions. As a result, these models are often estimated empirically using techniques such as orbital-phase scrambling, time-shifting of the ephemeris, or bootstrap resampling that preserves the temporal structure of the data while destroying long-term phase coherence.

Injection-recovery experiments play a dual role in this context. Beyond validating detrending, they define the sensitivity of the analysis to SPI-like signals. By injecting synthetic orbital-phase modulations, clustered flare populations, or spot-crossing anomalies across a grid of amplitudes and phases, one can construct detection-efficiency curves that quantify the probability of recovery given the data quality and analysis choices (Christiansen et al., 2016). In the absence of a detected signal, these curves provide robust upper limits on the amplitude or rate of any planet-linked photometric variability (Miller et al., 2012).

Population-level analyses offer an additional layer of statistical power (Mazeh et al., 2015). By comparing ensembles of stars with and without close-in planets, or by stacking phase-folded signals across multiple systems, marginal effects that are undetectable in individual light curves can be identified statistically. Such approaches require careful matching of control samples and explicit treatment of selection effects, but they can provide strong constraints on the prevalence of SPI (e.g. Ilin et al., 2024).

Chromospheric activity indexes

Chromospheric spectral lines are arguably the most widely used diagnostics of stellar magnetic activity (e.g. [Hall, 2008](#)) and have been prime targets in the search for SPI signatures. These lines are formed in the upper layers of the stellar atmosphere, where non-LTE conditions and magnetic energy dissipation become non-negligible (e.g. [Linsky, 2017](#)). The emission in the line cores is ultimately linked to the excitation and ionization of atoms in plasma whose thermodynamic state is strongly modulated by the local magnetic field. For this reason, chromospheric lines provide a more direct probe of magnetically driven variability than RVs, line-shape diagnostics, or photospheric observables.

We review the spectral lines and methods traditionally used to quantify chromospheric activity, and then consider how these diagnostics are adapted or reinterpreted in the context of SPI.

Ca II H & K lines

The most well-known chromospheric activity indicator is the Ca II H & K doublet. It was used to study the long-term activity evolution of solar-neighbourhood stars in the foundational work of [Wilson \(1978\)](#). The two lines are located at 393.3664 nm and 396.8470 nm and can be detected from a spectral resolution of $R \sim 10\,000$ due to their intrinsic width. Since RV planet-hunting spectrographs typically have $R \geq 60\,000$ and cover (traditionally) the visible range, one is capable of measuring these lines from RV campaign spectra, allowing an activity characterization contemporaneous with RV measurements (e.g. [Boisse et al., 2011](#)).

The activity index $\log(R'_{\text{HK}})$ defined by [Noyes et al. \(1984\)](#) remains in widespread use today, which attests to its effectiveness. Several teams have adapted the index to use in modern instrumentation (e.g. [Lovis et al., 2011](#)) or to extend to M-dwarf stars (e.g. [Suárez Mascareño et al., 2015](#)), but its underlying principles remain essentially unchanged. The flux in the line cores is measured and normalized by the nearby continuum. This ratio is then calibrated as a function of spectral type (often via $B - V$), in order to remove the photospheric contribution and yield a value that can be compared across stars of different spectral class.

Reported SPI detections, so far, have been based on detections in the Ca II lines. In the context of these studies, the analysis of the lines is done differently from the traditional $\log(R'_{\text{HK}})$ described above. In most SPI studies, the H and the K lines are treated separately; no index is calculated, but a variability measurement is done directly in the line core. For that, a bandpass of 7Å is centred around each line core. In order to normalise the spectrum, the ends of the bandpass are set to 1 (see, e.g. [Shkolnik et al., 2003, 2005, 2008a](#)). An average profile is then calculated from all observations, and the residual profile per observation is calculated by subtracting the average profile from the line core (within the bandpass). In principle, the residual profiles should only show variability in the core of the Ca line, and the edge of these profiles should be zero (within their error bars). In order to make sure that only the variability in the core is considered, some authors have corrected the residual profiles from possible continuum variability by subtracting a low order polynomial from the residuals (an offset correction as defined in, e.g. [Cauley et al., 2018](#)). Once the final residuals profiles are calculated (whether the last correction step is added or not), the flux in the core of the line is measured, and its variability is investigated for modulation with periods associated to SPI. [Figure 1](#) summarises the steps followed for the calculation of the index. We note here that some studies have combined the information from both the Ca II H & K lines (see, e.g. [Fares et al., 2009, 2010, 2012; Klein et al., 2022](#)), while others used the traditional index definitions.

A very recent study of the warm Neptune GJ 436 b reports evidence for magnetically-driven SPI traced through the Ca II H & K lines and the Ca infrared triplet ([Revilla et al., 2026](#)). The authors identify a periodic modulation of the host star’s activity on the timescale of the planet’s synodic and anti-synodic periods on top of the stellar rotation one. The signal is independently recovered with both HARPS and CARMENES, and shows an on-off behaviour, being detectable when the star is in an intermediate activity state of its long-term activity cycle. This result provides a rare indirect constraint on the magnetic field of a Neptune-mass exoplanet and extends SPI studies beyond the hot-Jupiter population.

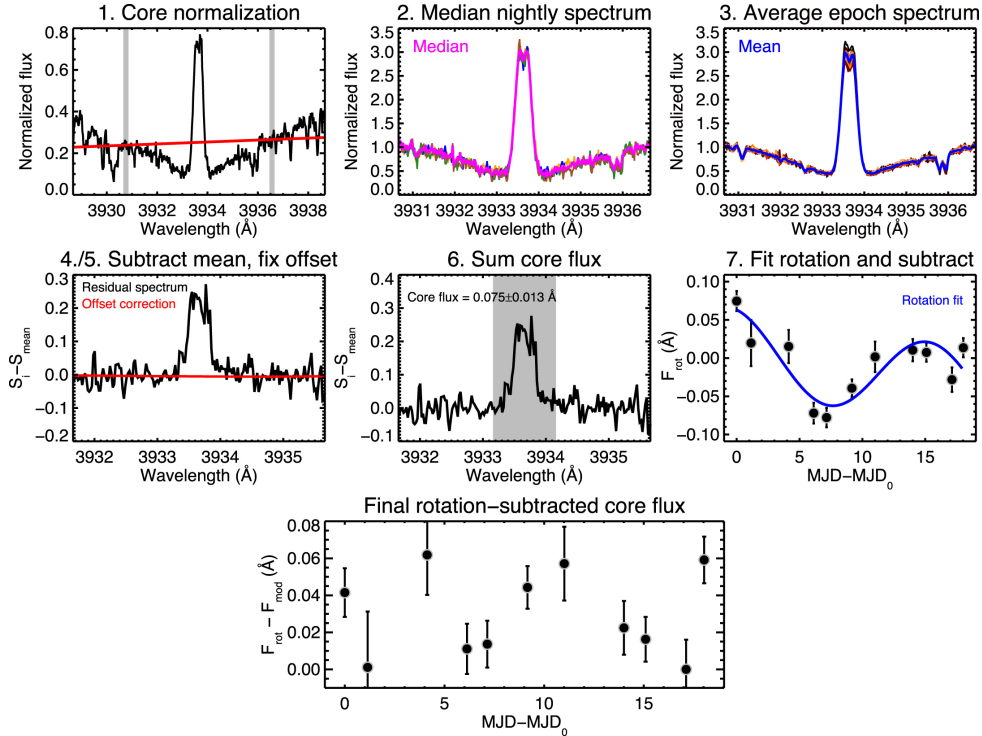


Figure 1: The derivation of the Ca II K flux, from [Cauley et al. \(2018\)](#). See text for details.

H α

The H α line (located at 656.28 nm) is a fundamental diagnostic of chromospheric magnetic activity, particularly in late-type stars, where its emission strength and profile changes reflect non-thermal heating processes associated with features such as plages, filaments, and flares ([Linsky, 2017](#); [Fuhrmeister et al., 2019](#); [Kuridze et al., 2015](#)). Although both H α and the Ca II H&K resonance lines are primary diagnostics for stellar magnetic activity, their inter-relationship is complex and frequently reveals significant discrepancies. These differences arise because the two tracers probe distinct atmospheric heights: Ca II H&K form in the middle-to-lower chromosphere, while H α originates in the upper chromosphere ([Gomes da Silva et al., 2011](#); [Linsky, 2017](#)). Consequently, they respond differently to magnetic structures; while *plages* generally produce a positive correlation in both lines, *filaments* can introduce negative or anti-correlated signals in H α ([Meunier et al., 2022](#)).

Beyond these discrepancies, one advantage of the H α line is its location in the red part of the optical spectrum, where it is generally easier to observe at high S/N than Ca II H & K, particularly in the cool M dwarf stars that became the focus of many RV surveys. This made the line an attractive activity tracer in RV campaigns and, by extension, in SPI studies. As with Ca II H & K, the usual approach is to measure the flux in the line core relative to nearby continuum bands, thereby defining an H α activity index. The bandwidth used to calculate the H α index is critical for its agreement with Calcium. In solar-type stars, an optimized 0.6 Å bandwidth focuses on the core emission and maximizes the positive correlation with Ca II, whereas the standard 1.6 Å filter incorporates variability from the line wings that can mask rotational signals or generate artificial “anti-cycles” ([Gomes da Silva et al., 2022](#)). For M dwarfs, the discrepancies are further accentuated because the Ca II flux is often extremely low and noisy in the blue spectral region ([Fuhrmeister et al., 2019](#); [Meunier et al., 2024](#)).

The interpretation of H α is often more nuanced than $\log(R'_{HK})$. Its response to magnetic activity depends appreciably on several parameters beyond spectral type, to the extreme that the line may appear either in absorption or emission depending on the physical conditions in the chromosphere. In low-activity stars, H α may show weak or even no detectable correlations with Ca II H & K, whereas in more active stars it can become a sensitive tracer of plages, flares, and transient chromospheric variability (e.g. [Cincunegui et al., 2007](#); [Gomes da Silva et al., 2011](#); [Ibañez Bustos et al., 2023](#)). Specifically in M dwarfs, H α activity—quantified by its fractional luminosity ($L_{H\alpha}/L_{bol}$)—exhibits

a uniquely non-linear evolutionary path. As rotation rates and activity levels increase, the line first deepens in absorption before “filling in” and eventually transitioning into full emission (Newton et al., 2017). During high-energy flare events, this transition from absorption to emission can occur rapidly (Namekata et al., 2022). Such sensitivity to both quiescent and transient chromospheric states necessitates extreme caution when interpreting orbit-phased or intermittent modulation as evidence of SPI.

He I

The He I line most commonly used as an activity diagnostic in optical spectra is the He I D₃ triplet, located near 587.6 nm. In cool stars, this line forms in the upper chromosphere and lower transition region, and its appearance is closely linked to non-radiative heating and high-energy irradiation (Andretta and Giampapa, 1995). Unlike traditional resonance lines such as Ca II H & K or the H α Balmer line, the formation of the He I D₃ triplet in late-type stars is primarily driven by a photoionization-recombination (PR) mechanism (Andretta and Giampapa, 1995; Sanz-Forcada and Dupree, 2008).

Consequently, He I serves as a more selective tracer of energetic atmospheric processes than traditional indicators. While Ca II and H α reflect the bulk properties of the mid-to-lower chromosphere, and upper chromosphere, respectively, He I acts as a direct proxy for the high-energy radiation field and the presence of highly localized heating events (Sanz-Forcada and Dupree, 2008; Guilluy et al., 2020). In practice, the line is typically quantified through indices based on its core flux or equivalent width (EW) measured relative to the local continuum. However, the observational implementation of He I as a tracer remains demanding. In inactive stars, the line is inherently weak and frequently contaminated by telluric absorption features or blended with nearby metallic lines, necessitating high-resolution spectra and meticulous data reduction (Guilluy et al., 2020; Fuhrmeister et al., 2019) for a proper analysis. Furthermore, its response is non-linear; the line can appear in absorption, “filling-in”, or transitioning into emission depending on the specific thermal structure and radiation field of the upper atmosphere (Andretta and Giampapa, 1995). Despite these complexities, its unique sensitivity to the most energetic layers of the stellar atmosphere makes it exceptionally attractive for studying Star-Planet Interaction (SPI). In systems with close-in exoplanets, magnetic or particle-driven interactions—such as reconnection events or the formation of bow shocks—preferentially impact the upper chromosphere, potentially creating sub-orbital signatures in He I that remain distinct from the background stellar activity (Guilluy et al., 2020).

Na I

The Na I D doublet, located at 588.9950 nm and 589.5924 nm, is also commonly used as an activity diagnostic in cool stars. Although these lines are primarily photospheric in origin, their deep, narrow cores are formed in the lower-to-middle chromosphere, making them sensitive to non-thermal heating and magnetic activity (Andretta and Giampapa, 1995; Montes et al., 1997). In active stars, this sensitivity manifests as a central emission within the absorption cores, a process that can be quantified through activity indices defined by measuring the core flux relative to nearby continuum passbands, analogous to the methods used for Ca II H&K and H α (Díaz et al., 2007).

A primary observational advantage of the Na I D lines is their location in the yellow-red portion of the optical spectrum. For cool M dwarfs, which exhibit drastically reduced flux in the blue-UV region, the Na I doublet provides a high signal-to-noise (S/N) alternative to the traditional Ca II H&K (Díaz et al., 2007; Fuhrmeister et al., 2019). This makes the doublet a staple in large-scale radial velocity (RV) surveys and long-term activity monitoring programs where blue-channel sensitivity may be limited. However, the interpretation of Na I activity is rarely straightforward (Meunier et al., 2024). The lines retain a substantial photospheric contribution, which must be carefully accounted for to isolate the chromospheric signal. Furthermore, the doublet is frequently affected by telluric water vapour absorption and interstellar medium (ISM) contamination; the latter is particularly problematic as ISM absorption features can overlap with the stellar line cores depending on the target’s radial velocity (e.g., Welsh et al., 2010; Díaz et al., 2007).

In Star-Planet Interaction (SPI) studies, Na I provides a critical complementary diagnostic. Because it probes a transition region between the upper photosphere and the lower chromosphere, it offers a different perspective on the atmospheric response to planetary perturbations compared to the higher-forming H α or He I lines. This mixed sensitivity allows for a more comprehensive “tomography”

of the stellar atmosphere during suspected SPI events (e.g., [Cauley et al., 2018](#)). Nevertheless, the complexity of its formation requires caution, as observed modulations in the Na I index may reflect a combination of photospheric spots and chromospheric plages rather than a purely planet-induced signal ([Klein et al., 2022](#); [Ibañez Bustos et al., 2023](#)).

Taken together, these diagnostics probe different layers and physical regimes of the stellar atmosphere, from the lower chromosphere to the upper chromosphere and transition region. Their simultaneous use is therefore particularly valuable in SPI studies, where the expected signal may be weak, intermittent, and manifest differently depending on the atmospheric depth and physical mechanism involved. Unfortunately, the characteristics of the star and properties of the spectra may make a multi-index analysis impractical.

Radio observational diagnostics of magnetic SPI

Radio searches for magnetic star–planet interaction (SPI) have evolved from the initial, simple flux-density searches for exoplanetary cyclotron emission in the early 90s to multi-dimensional searches based on polarization, time–frequency behaviour, planetary orbital phase, and stellar activity context. The physical basis remains the Solar-System analogy established by [Zarka \(2007\)](#): a plasma flow interacting with a magnetized or conducting obstacle can drive electron acceleration and coherent electron-cyclotron maser (ECM) emission. In direct planetary emission, the relevant magnetic field is the planetary field and the maximum frequency is

$$\nu_c \simeq 2.8 B \text{ MHz}, \quad (4)$$

where B is in Gauss. This immediately imposes a strong observational selection effect: terrestrial planets with Gauss-level fields emit below or close to the ionospheric cut-off, whereas hot Jupiters or strongly magnetized planets may reach the decametre–metre window. In sub-Alfvénic SPI, however, the emission can be produced in the stellar magnetosphere, so the relevant field is the stellar coronal field. For active M dwarfs, with surface fields of hundreds of gauss to kilogauss, the predicted ECM frequencies move into the LOFAR/uGMRT/VLA/ATCA range, from tens of MHz to several GHz ([Zarka, 2007](#); [Saur et al., 2013](#); [Turnpenney et al., 2018](#); [Vedantham et al., 2020](#); [Pérez-Torres et al., 2021](#); [Callingham et al., 2024](#)).

The main observational advance has therefore been methodological rather than simply instrumental. A credible radio SPI experiment now requires simultaneous or sequential tests of: (i) coherent-emission diagnostics, especially high circular polarization and high brightness temperature; (ii) time-domain behaviour, including bursts, persistence, duty cycle, and dynamic spectra; (iii) frequency placement relative to plausible cyclotron frequencies; (iv) phase coherence with the orbital or synodic period; and (v) rejection of ordinary stellar activity through chromospheric, coronal, rotation, and flare information. None of these criteria is individually decisive, but together they define the current evidentiary standard for candidate magnetic SPI.

From targeted low-frequency searches to Stokes- V survey selection

The first generation of exoplanet radio searches was motivated by the radiometric Bode-law and radio-magnetic scaling-law extrapolations from Solar-System planets ([Zarka, 2007, 2018](#)). Observations targeted systems expected to maximize incident stellar-wind power, planetary magnetic moment, or proximity, often at low frequencies where Jovian analogues should be brightest. The observational limitations were severe: ionospheric access, radio-frequency interference, uncertain beaming, poor knowledge of planetary magnetic fields, and the possibility that the stellar wind or planetary plasma environment suppresses ECM escape ([Turner et al., 2021](#); [Callingham et al., 2024](#)). Consequently,

many searches have produced upper limits rather than detections, and non-detections were difficult to interpret uniquely.

The advent of instruments working at very low frequencies and with enormous sensitivities, such as LOFAR, enabled sensitive, blind wide-field imaging in both total intensity and circular polarization rather than pointing only at pre-selected exoplanet systems. [Vedantham et al. \(2020\)](#) identified GJ 1151 by cross-matching LoTSS sources with nearby Gaia stars. The source was detected at 120–167 MHz with a high circularly polarized fraction, persistent emission over an ~ 8 h observation, and a quiescent chromospheric activity state. Its brightness temperature and polarization argued against incoherent gyrosynchrotron emission, while plasma emission was disfavoured by the combination of polarization and coronal-density constraints. The remaining interpretation was auroral ECM powered by a large-scale current system, plausibly a sub-Alfvénic interaction with a short-period planet ([Vedantham et al., 2020](#)). However, since no close-in planet has been detected in the system, nor has LOFAR confirmed the emission in subsequent observations, the SPI interpretation remains simply a possibility.

This approach was generalized by [Callingham et al. \(2021\)](#), who used LoTSS Stokes- V maps and Gaia cross-matching to build a blind sample of 19 low-frequency M-dwarf detections. Most sources displayed high circular polarization, brightness temperatures above 10^{12} K, broad effective bandwidths, and hour-scale persistence. The important methodological result was the population comparison: radio luminosity did not correlate cleanly with standard chromospheric or coronal activity indicators, and slowly rotating, X-ray faint stars became the cleanest SPI candidates. Thus, survey selection in Stokes V provides a way to find systems where the radio emission is not simply tracing ordinary flare activity, although it does not by itself prove the presence of a planet.

Targeted monitoring of known planet hosts

A complementary method is phase-resolved monitoring of known close-in planet hosts. The most developed example is the ATCA campaign on Proxima Centauri by [Pérez-Torres et al. \(2021\)](#). The experiment used 18 consecutive daily observations from 1.1 to 3.1 GHz, covering about 1.6 orbital cycles of Proxima b. The observing frequency was chosen because the stellar magnetic field of Proxima, $B_{\star} \simeq 600$ G, implies an ECM frequency near 1.7 GHz if the emission arises in the stellar magnetosphere. The analysis combined full-Stokes imaging, frequency-resolved flux measurements, short-timescale searches in the visibility domain, and folding of the radio light curve on the known planetary orbit. The key diagnostics were the strong low-frequency component around 1.6 GHz, high circular polarization, reversals of the Stokes- V sign, short flares, and a multi-day burst with maxima close to the quadratures of Proxima b. The interpretation remains a candidate rather than a confirmed detection, but it established the template for GHz-frequency SPI monitoring: select the band from the stellar magnetic field, monitor long enough to test orbital phase, and use polarization plus spectral cut-offs to discriminate ECM from plasma emission or gyrosynchrotron radiation.

The same logic has been applied to other nearby M-dwarf planet hosts. [Pineda and Villadsen \(2023\)](#) reported 2–4 GHz coherent bursts from YZ Ceti, with repeated bursts occurring at similar orbital phases of YZ Ceti b, consistent with enhanced burst probability near the predicted SPI phase, while retaining caution about intrinsic stellar bursts. [Trigilio et al. \(2023\)](#) used uGMRT Band 4 observations of YZ Ceti and argued, from repeated detections, circular polarization, and orbital-phase statistics, for auroral emission associated with SPI. These works show why phase-resolved monitoring is now central: a single polarized burst demonstrates coherent emission, but periodic recurrence at the planet’s orbital or synodic phase is what turns a stellar-radio detection into an SPI candidate.

Non-detections are equally important when they are obtained with complete phase coverage and appropriate Stokes- V sensitivity. [Narang et al. \(2024\)](#) re-observed GJ 1151 with the uGMRT at 150, 218, and 400 MHz and did not recover the LOFAR-like emission, emphasizing that SPI candidates may be intermittent, beamed away from the observer, absorbed, or active only under favourable stellar-wind conditions. [Peña-Moñino and Pérez-Torres \(2025\)](#) carried out nine uGMRT epochs of GJ 486 from 550 to 750 MHz, covering almost the full orbital phase of GJ 486b. The observations produced no Stokes- I or Stokes- V detection and no burst in dynamic spectra. Because the band was selected from the expected stellar ECM frequency, the non-detection could be translated into constraints on the stellar mass-loss rate, radio conversion efficiency, and beaming geometry. This illustrates a newer use of radio SPI observations: even non-detections can constrain the allowed parameter space if the campaign has adequate orbital coverage, polarization products, dynamic spectra, and a forward model including the stellar wind, magnetopause size, and free-free absorption.

Dynamic spectra, polarization, and mechanism discrimination

The core data product for SPI searches is no longer only a continuum image but a set of Stokes- I and Stokes- V images, light curves, and dynamic spectra. Imaging is needed to verify positional association and remove unrelated background sources. Stokes V is crucial because coherent ECM can approach very high circular polarization, whereas most incoherent stellar emission is weakly polarized. Dynamic spectra are needed because ECM may appear as narrowband or structured bursts that are diluted in time-averaged imaging. They also allow searches over several time and frequency binnings, which is essential when the intrinsic burst duration and bandwidth are unknown (Peña-Moñino and Pérez-Torres, 2025).

The main ambiguity is between ECM and coherent plasma emission. Plasma emission can also be bright and polarized, particularly in active coronae, but it is tied to the plasma frequency and its harmonics, depends strongly on coronal density, and often has different polarization and time–frequency behaviour. ECM is tied to the cyclotron frequency, requires low plasma-to-cyclotron frequency ratios along the escape path, and is expected to be beamed. Practical discrimination therefore uses a combination of observables: very high brightness temperature, high circular polarization, spectral cut-offs consistent with ν_c , stable polarization handedness or hemisphere-dependent reversals, hour-scale auroral persistence, and recurrence at orbital phase (Vedantham et al., 2020; Pérez-Torres et al., 2021; Callingham et al., 2021, 2024). Ancillary optical, $H\alpha$, X-ray, rotation, and magnetic-field measurements are required to decide whether the source is a normal active star, a rotation-powered auroral emitter, or a plausible planet-induced system.

Current best practice and remaining limitations

The current best practice for radio SPI searches is therefore a matched observing and modelling workflow. First, targets are selected among nearby M dwarfs or known close-in planet hosts for which the expected cyclotron frequency is accessible and the planet may orbit inside the Alfvén surface. Second, observations are designed to cover the relevant orbital and synodic phases, ideally over multiple cycles, with full-Stokes products and sufficient time–frequency resolution to form dynamic spectra. Third, candidate detections are evaluated against a hierarchy of tests: positional coincidence, high Stokes- V fraction, brightness temperature, spectral behaviour, recurrence, orbital/synodical-phase clustering, and absence of ordinary stellar-activity counterparts. Finally, detections and non-detections are interpreted with forward models of the sub-Alfvénic interaction, beaming, stellar magnetic geometry, stellar wind density, and propagation losses (Saur et al., 2013; Turnpenney et al., 2018; Callingham et al., 2024; Peña-Moñino and Pérez-Torres, 2025).

The field has not yet reached the level of an unambiguous, repeatable radio detection of magnetic SPI. The leading candidates show several of the expected signatures, but the evidence is limited by beaming, intrinsic intermittency, stellar flare contamination, incomplete knowledge of the stellar wind, and sparse repetition of orbital phase coverage. The methodological progress is nevertheless substantial. Radio SPI searches have become quantitative tests of magnetospheric electrodynamics rather than simple source searches, and the combination of LOFAR, uGMRT, VLA/ATCA monitoring, optical radial velocities, magnetic mapping, and future LOFAR 2.0/SKA-Low sensitivity should make it possible to distinguish persistent stellar aurorae, stochastic coherent flares, direct planetary aurorae, and genuine planet-induced radio emission.

Transmission spectroscopy

The interaction between a planet and its host star leaves various imprints on the planet’s atmosphere. These interactions are driven by processes that include, mainly, the deposition of stellar radiation on the planet, the interception of the planetary wind by its stellar counterpart, and the coupling of the planetary outflow with the star-planet magnetic environment. Most efforts to characterize exoplanet atmospheres take advantage of such interactions which, under appropriate conditions, make the atmospheric signatures more readily detectable. Furthermore, there is an increasing interest in using a few specific atmospheric tracers to constrain the stellar properties, a goal that requires a sound understanding of the processes behind star-planet interactions.

Among the techniques used for the characterization of exoplanet atmospheres, transmission spectroscopy has been the most successful to date. The atmosphere is revealed through the difference in the joint star-planet spectra measured while the planet is transiting its host star relative to the spectrum while the planet is off transit. Because the transit probability is inversely proportional to orbital distance, transmission spectroscopy is best suited for the study of close-in exoplanets. This constraint prevents its use in the characterization of the vast majority of exoplanets, including Proxima Centauri b – the nearest to us, and which orbits the habitable zone (HZ) of its host star (Anglada-Escudé et al., 2016; Jenkins et al., 2019). On the other hand, the proximity of most star-planet systems studied using transmission spectroscopy often leads to enhanced star-planet interactions and stronger atmospheric signatures. The signatures of the chemical species searched for with transmission spectroscopy will be strong if the species are abundant and their cross sections large. For example, the cross sections of dipole-allowed atomic lines can be as large as 10^{-13} cm² at the line’s core, enabling the detection of major species out to far distances from the planet, and of minor species to altitudes similar to the planet’s optical radius. By targeting multiple lines of the same or different species, transmission spectroscopy renders possible the investigation of star-planet interactions over a range of conditions and altitudes in the planet’s atmosphere. In short, transmission spectroscopy is a unique tool to explore the composition, temperature and dynamics of an atmosphere and their connection with the stellar environment.

To illustrate these possibilities, we focus on the H I Lyman- α line at 1,216 Å, the H I Balmer, the C II resonance line at 1,335 Å and the He I triplet line at 1.08 μ m. They trace the low-density atmospheric layers in the upper atmosphere where the interaction with the star is stronger. For the gas to reach such altitudes, and possibly escape the planet’s gravitational pull, the planet must receive large amounts of stellar radiation. Stellar XUV photons (of wavelengths less than the Lyman continuum threshold at 912 Å) are crucial to photoionize the H I atoms, often prevalent at high altitudes, and heat the atmosphere as the ejected primary electrons transfer their kinetic energy to the gas (Cecchi-Pestellini et al., 2006; García Muñoz, 2023). Unfortunately, the XUV spectra of most stars are poorly known because it is masked by the interstellar medium. Much work is being done to fill in this critical gap, which often requires extrapolations based on reference stars or the reconstruction of the stellar corona from measurements of the stellar flux at X-ray and FUV wavelengths (Youngblood et al., 2016; Wilson et al., 2025). The detection of these lines requires moderate-to-high spectral resolution, typically $\lambda/\Delta\lambda > 1,000$ and a bright stellar background. Both requirements are more easily met at visible and infrared wavelengths, as many medium and large-size ground-based telescopes are equipped with high-resolution spectrographs, like CRIRES+, NIRPS, CARMENES, GIANO and SPIRou. For lines at wavelengths shorter than the ozone cutoff of $\sim 3,100$ Å, observing from space is a must. Indeed, UV transmission spectroscopy of exoplanets has mostly relied on the Hubble Space Telescope. Ensuring the availability of space telescopes capable of UV spectroscopy of exoplanets to build upon HST’s legacy should remain a priority. The proposed Habitable Worlds Space Observatory and other international ventures (Gómez de Castro et al., 2022; Cubillos et al., 2025; Dos Santos et al., 2025) will supersede HST in the mid-term.

In absorption, the H I Lyman- α line arises in the dipole-allowed transition $H(1s) + h\nu(1,216 \text{ Å}) \rightarrow H(2p)$. The abundance of H I atoms in the atmospheres of the close-in gas giants targeted in early transmission spectroscopy surveys led to the rapid detection of the line (Vidal-Madjar et al., 2003). On the well-known hot Jupiter HD 209458 b, the line remains opaque over at least $\sim \pm 100$ km/s from line core, that corresponds to a projected area equivalent to a few times the planet’s optical radius (Vidal-

Madjar et al., 2003; Linsky et al., 2010). Models indicate that hydrogen is lifted to such high altitudes by strong XUV irradiation from its Sun-like host star (Yelle, 2006; García Muñoz, 2007). At the also well-known hot-Jupiter HD 189733 b, absorption in the H I Lyman- α line has been reported to fluctuate over time (Lecavelier Des Etangs et al., 2010; Lecavelier des Etangs et al., 2012), becoming strong at some epochs while going undetected at others. This temporal variability in the planet’s atmosphere is likely an outcome of variability in the radiative output or the wind properties of the host star (Cheremkov et al., 2017; Hazra et al., 2022). This connection offers a means of probing the stellar properties, including the magnetic field (Khodachenko et al., 2021), from their effects on the planet atmospheres. For these mechanisms to be truly effective and make a detectable impact, however, they must last at least a time of a few hours comparable to that of the transit duration (Cheremkov et al., 2017; Hazra et al., 2022; Gillet et al., 2025).

Arguably, the most intriguing detections of H I Lyman- α line absorption are those on the Neptune-sized GJ 436 b, GJ 3470 b, and HAT-P-11 b (Kulow et al., 2014; Bourrier et al., 2018; Ben-Jaffel et al., 2022). All three planets show evidence for envelopes of H I atoms out to many times their optical radii (Fig. 2) that mask large fractions of their host star disks. Given the strong measured signal brightness of the host stars, temporally-resolved spectroscopy is feasible, thereby enabling unique physical insight. For GJ 436, the most extensively investigated of these planets, the transmission spectrum is highly asymmetric, with absorption at blue (short) wavelengths typically stronger than at red (long) wavelengths. This has been interpreted as resulting from a long tail of H I atoms that trails the planet at line-of-sight velocities of at least 120 km/s. The three-dimensional shape of this H I envelope is presumably responsible for the specifics of the light curve (especially at blue wavelengths), which exhibits a sharp ingress but a very long egress (Lavie et al., 2017). The atmospheric models that have attempted to reproduce the richness of the measured temporally-resolved spectra have mostly focused on the multi-dimensional dynamics of the planetary and stellar winds under the effects of stellar radiation and ram pressure, charge exchange between the stellar wind protons and the planetary neutrals, photoionization and the simultaneous gravitational pull from both the star and the planet (Khodachenko et al., 2019; Villarreal D’Angelo et al., 2021). Although some published models reproduce reasonably well the main features of the measurements (possibly tuning the stellar XUV output and stellar wind properties), other features such as the egress light curve shape at red wavelengths have demonstrated to be difficult to model, a difficulty that suggests that some physics in the star-planet interaction of the models is missing. The fact that the relative importances of stellar radiation and ram pressure, and charge exchange, is not entirely clear serves also as a warning that the star-planet interactions driving the strength of the H I Lyman- α line are not fully understood yet. More work is needed, in particular to understand the atom-scale details of charge exchange and the significance of diffuse Lyman- α radiation – effects that have so far been overlooked.

There has been recent interest in using the H I Lyman- α line to explore sub-Neptune-sized exoplanets, thus complementing transmission spectroscopy observations at longer wavelengths and that probe the deeper atmospheres. The attempts to detect the absorption signature of this line on planets smaller than $3R_{\oplus}$ include π Men c, TRAPPIST-1 b & c, HD 97658 b, Kepler-444 e, GJ 1132 b, 55 Cnc e, HD 63433 b & c, GJ 9827 b, and TOI-776 b & c. Except for TOI-776 b & c (Lloyd et al., 2025), all these detection attempts have failed, which has been puzzling because strong signatures are expected if the planet atmospheres are hydrogen-dominated. This is indeed the case of π Men c ($2.1R_{\oplus}$, $4.5M_{\oplus}$), which orbits its Sun-like star every 6.3 days. A single-transit observation of this object (García Muñoz et al., 2020) with the HST/STIS instrument (Fig. 2) revealed no evidence of in-transit absorption even though the data are of high quality. Three-dimensional modelling of the system shows that the non-detection can only be explained by a stellar wind notably weaker than solar, an XUV higher than estimated from the available X-ray data or a combination of these two conditions (Shaikhislamov et al., 2020). The non-detection might also be explained if the atmosphere is not hydrogen dominated, which would reduce the escape rate and accelerate the transition in the planetary wind from neutral into ionized hydrogen (García Muñoz et al., 2020). The idea of a volatile-rich atmosphere is reinforced by the fact that the retention time of a hydrogen-dominated atmosphere on π Men c is much shorter than its age (~ 5 Gyr). Observations of π Men c at optical and infrared wavelengths, in particular with JWST, ARIEL (Tinetti et al., 2018) or from the ground, have the potential to shed new light on the nature of this planet and in turn other sub-Neptunes.

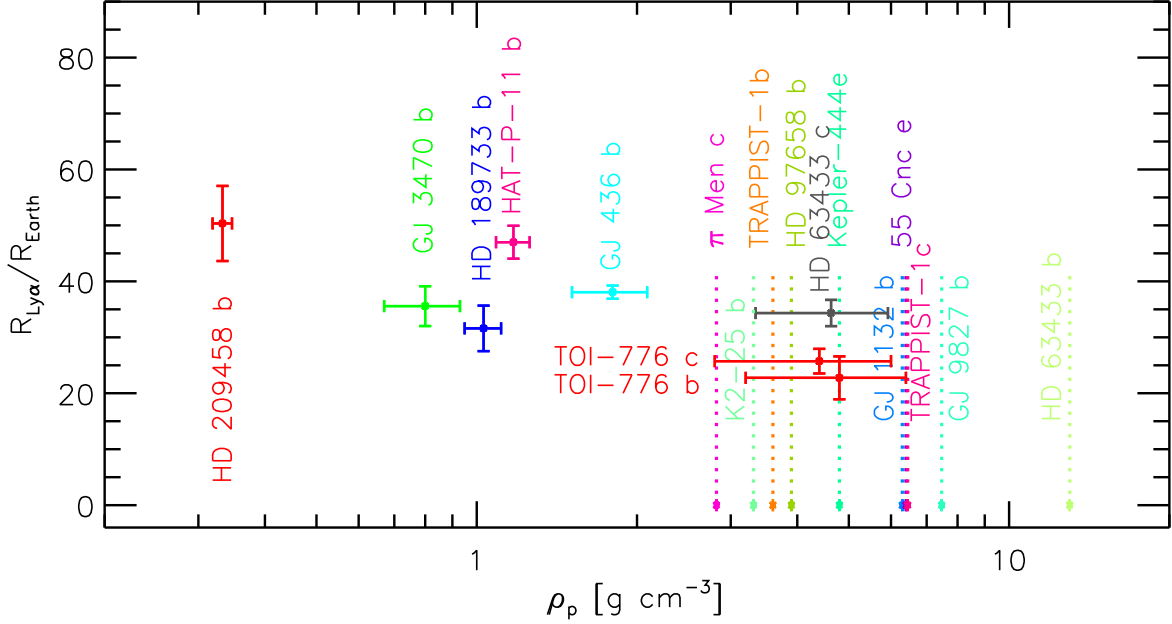


Figure 2: Summary of detection attempts of H I Lyman- α absorption on exoplanets. Figure based on [García Muñoz et al. \(2020\)](#), and updated with recent observations. The measured transit depths have been translated into effective Earth sizes.

A few lines of the H I Balmer series, $H(n=2)+h\nu\rightarrow H(n\geq 3)$, where n stands for principal quantum number, have been detected on a few ultrahot Jupiters with equilibrium temperatures $>2,000$ K ([Yan and Henning, 2018](#); [Czesla et al., 2022](#)), some of them orbiting early-type stars. According to models, the absorbing excited state $H(n=2)$ is populated by either Lyman- α radiation (stellar plus diffuse) or by collisions of $H(n=1)$ with thermal electrons when the gas temperature is sufficiently high ([Yan et al., 2021](#)). For the extreme KELT-9b ($T_{\text{eq}}\sim 4,000$ K) models show that the excited state $H(n=2)$ (ionization potential of 3.4 eV) plays a key role in the ionization and heating of the atmosphere under the strong near-UV irradiation conditions of its A-type host star ([García Muñoz and Schneider, 2019](#)). KELT-9b represents an exception, although possibly not the only one, in that the stellar near-UV spectrum may be more important than at least as important as its XUV counterpart at governing the specifics of the atmospheric outflow. Temporal variability during transit in some of the atmospheric lines detected on this planet have been tentatively ascribed to a flare ([Cauley et al., 2019](#)), challenging the common belief that A-type stars do not exhibit such events. Subsequent observations have not confirmed this possibility ([Wyttenbach et al., 2020](#)). Unlike the H I Lyman- α line at 1,216 Å, those in the Balmer series are largely unaffected by the terrestrial atmosphere and can be observed from the ground at high spectral resolution. The lines are usually resolved over the core and wings, and the existence of multiple of these, each with a different strength as dictated by their specific oscillator strengths makes the Balmer series sensitive to a range of atmospheric altitudes. There are several hints that some of the H I Balmer lines might be Doppler-shifted with respect to star rest frame (Fig. 25 of [Sánchez-Lavega et al. \(2023\)](#)). Indeed, the significant width of the lines makes it difficult to extract any information concerning the preferential motion of the absorbing gas either towards the observer or the star.

What is commonly called the C II “resonance line” at 1,334/1,335 Å is actually a triplet. The component at 1,334 Å is often masked by ISM absorption, with the two components at 1,335 Å overlapping and being in practice undistinguishable. There is some evidence for the presence of this line in the atmospheres of HD 209458 b ([Vidal-Madjar et al., 2004](#)), π Men c ([García Muñoz et al., 2021](#)) and HAT-P-11 b ([Ben-Jaffel et al., 2022](#)). Neutral carbon (IP=11.3 eV) becomes rapidly photoionized under the stellar irradiation conditions of close-in exoplanets. The photoionization lifetime of C II (IP=24.4 eV) is however much longer, which ensures that once formed the C II ion may travel far

in the atmosphere and is largely unaffected by radiation, potentially building up a large absorbing column in the line-of-sight direction. This is essentially the idea used to rationalize the detections on both π Men c and HAT-P-11 b of C II with velocities of up to 70 km/s away from the star. As an ion, the C II dynamics and therefore its corresponding line strength is sensitive to the magnetic environment near the planet, as shown by combined hydrodynamic and Particle-In-Cell simulations (Ben-Jaffel et al., 2022).

Transmission spectroscopy in the He I triplet line at 1.08 μm has emerged in the last years as a valuable means of exploring the upper atmospheres of close-in exoplanets. The line is formed in the dipole-allowed transition $\text{He}(2^3S)+h\nu(1.08 \mu\text{m})\rightarrow\text{He}(2^3P)$ that connects the metastable state $\text{He}(2^3S)$ with the next excited state in the triplet manifold. The $\text{He}(2^3S)$ population in the atmosphere is typically very small, but the large cross section of the transition at the line core and strong stellar background in the infrared make the line detectable at high resolution. The He I triplet line is indeed an ideal target for observations from the ground with moderate-to-large telescopes equipped with high-resolution spectrographs.

The $\text{He}(2^3P)$ state is populated by radiative recombination of the precursor He II ion, as in $\text{He}^++e^-\rightarrow\text{He}(i)+h\nu$ and subsequent de-excitation of the nascent excited states $\text{He}(i)$ (Oklopčić and Hirata, 2018). Large amounts of $\text{He}(2^3S)$ are formed in the collision of non-thermal electrons with ground state $\text{He}(1^1S)$, but this process is usually only the dominant one too deep in the atmosphere to be detectable in the transmission spectrum (García Muñoz, 2025). The $\text{He}(2^3S)$ loss is controlled by a variety of processes. Photoionization by stellar photons of wavelengths shorter than 2,600 Å is potentially important (Oklopčić, 2019), even if the predictions based on it do not fully match observations (Guilluy et al., 2024). Penning ionization, where the energy of the excited state $\text{He}(2^3S)$ is used to eject an electron from a hydrogen atom, is also important (García Muñoz, 2025).

Interestingly, the He I triplet line at 1.08 μm has been detected in a few Neptune- and sub-Neptune-sized planets (Guilluy et al., 2024). The latter group includes GJ 3090 b ($\sim 2.1R_{\oplus}$, Ahrer et al., 2025). The correct interpretation of the line presence is particularly important for these objects, which often lack any other signatures in their optical and infrared transmission spectra. On these planets, the removal of the precursor ion He^+ in collisions with H_2 at moderate temperatures acts as a efficient $\text{He}(2^3S)$ sink (García Muñoz et al., 2025). Omitting this process may bias any inferences on the He/H ratio in the planets’ atmospheres.

Like the H I Lyman- α line, the He I triplet line enables exploring the large-scale dynamics of the outflow. This is particularly important for planets such as the the ultrahot Jupiter HAT-P-32 b, which exhibit very extended (leading and trailing) tails traceable in the He I triplet line (Czesla et al., 2022; Zhang et al., 2023). For HAT-P-32 b and some other ultrahot Jupiters, the simultaneous detection of the He I triplet line and some H I Balmer lines provides complementary information to constrain the chemistry, dynamics and energetics of the gas. Unlike the H I Balmer lines, which so far have only been detected at ultrahot Jupiters, the He I triplet line has been identified on planets with very different equilibrium temperatures. The H I Balmer lines, the He I triplet line is also relatively narrow, which allows to determine its relative position with respect to the stellar rest frame. Many of the He I triplet line detections exhibit a net blue shift that suggests a day-to-night net motion of the $\text{He}(2^3S)$ atoms. According to models (Schreyer et al., 2024), the net offset may be sensitive to the strength of the near-planet magnetic field. If true, the measured offset would be revealing the planet’s magnetic field. For some planets such as the warm-Neptune GJ 3470 b, the strength of the He I triplet line seems to vary significantly over time (Guilluy et al., 2024; Masson et al., 2024). Model calculations show that the varying line strength is consistent with a possible rotational or cycle modulation in the stellar output from the host star (García Muñoz et al., 2025). The hypothesis should ideally be tested with simultaneous observations of the He I triplet line and the host star’s X-ray output. If proven correct, the available and future observations of the line might be used to monitor the stellar high-energy output.

While transmission spectroscopy provides a powerful probe of exoplanetary atmospheres and their coupling to the stellar environment, as discussed above, its interpretation is intrinsically limited by the fact that the observed signal is a convolution of planetary atmospheric absorption and the heteroge-

neous stellar photosphere. Stellar photospheric heterogeneities, such as starspots and faculae, introduce wavelength-dependent biases in transmission spectra through the so-called transit light source effect (TLSE, Rackham et al. (2018)), which can mimic or obscure atmospheric features and bias the inferred planet-to-star radius ratio. Recent studies have shown that simplified contamination models based solely on disk-averaged filling factors and spectral contrasts may fail to accurately reproduce the observed signal, particularly in the optical where limb darkening and transit geometry play a dominant role (Sumida et al., 2026). Self-consistent, pixel-resolved modeling demonstrates that these effects can lead to discrepancies of up to several hundred ppm, comparable to or larger than typical atmospheric signals, especially for active stars and non-equatorial transits. Moreover, attributing observed spectral slopes solely to stellar contamination may require unrealistically large and hot active regions, indicating that a combination of stellar and planetary contributions is often necessary to explain the data. These results highlight that reliable atmospheric characterization demands geometry-aware models of stellar heterogeneity that explicitly account for the spatial distribution of active regions and limb-darkening effects.

SPI detection in timeseries

Ultimately, the detection of SPI signatures relies on their unambiguous identification in time series measurements. Signal searches are often conducted by attempting to identify periodic or quasi-periodic modulations at characteristic timescales of the system, such as the planetary orbital period, the stellar rotation period, or the synodic period between the two.

These time series are typically analysed using generalized Lomb–Scargle (GLS) periodograms (Lomb, 1976; Scargle, 1982; Zechmeister and Kürster, 2009), which are well suited to the unevenly sampled data commonly acquired for planetary searches and characterization. In particular, a recurring modulation phased with the planetary orbit is often regarded as one of the most compelling signatures of SPI, and several methodological advances toward this goal have been developed in recent years.

Characteristic periods and pre-whitening

A fundamental preliminary step in any time-series search for SPI is the identification and removal of signals unrelated to the planet. The dominant timescale and mechanism of stellar variability is stellar rotation: active regions rotating in and out of view modulate the emission at the stellar rotation period, P_{rot} , and its harmonics. SPI-induced activity, by contrast, is not anchored to the stellar surface; instead, it is synchronized with the planet’s orbital motion and is therefore expected to be modulated at a period related to the planetary orbital period, P_{orb} (e.g. Shkolnik et al., 2003, 2005).

However, the SPI signal is not necessarily expected to appear exactly at P_{orb} . Considering the case of SPI measured through a chromospheric index, the interaction may preferentially occur onto localized chromospheric regions fixed in the stellar reference frame, while the observable modulation occurs at the synodic period of the system (Fares et al., 2010; Lanza, 2012):

$$P_{\text{syn}} = \left(\frac{1}{P_{\text{orb}}} - \frac{1}{P_{\text{rot}}} \right)^{-1}, \quad (5)$$

Depending on the geometry of the interaction, planets on polar or retrograde orbits may also exhibit a complementary frequency, the so-called anti-synodic period, $P_{\text{a-syn}} = (P_{\text{orb}}^{-1} + P_{\text{rot}}^{-1})^{-1}$ (Revilla et al., 2026). A search restricted to P_{orb} alone therefore risks missing the actual SPI signal, and periodogram analyses should generally explore the vicinity of all four characteristic periods.

Fischer and Saur (2019) proposed additional periods at which SPI signatures might manifest and that should therefore be considered in such searches. Depending on the system geometry and viewing angle, a signal may be observable at $P_{\text{syn}}/2$. Moreover, in systems hosting multiple planets within the Alfvén surface, each planet may generate its own Alfvén wing. Interactions between these wings could

then produce a signal with a characteristic period corresponding to the synodic period between the orbital periods of the planets involved.

The expected periodicity of the SPI signal also depends on the underlying interaction mechanism. Magnetic SPI is often expected to produce variability at the synodic period, or at related orbital frequencies, since the interaction is governed by the relative motion between the planet and the stellar magnetic field. However, magnetic SPI signatures may also appear at harmonics of the orbital period, including $P_{\text{orb}}/2$, for instance when the interaction geometry produces two maxima per orbit, as observed in radio studies of the Proxima Centauri system (e.g. Pérez-Torres et al., 2021), in analogy with the Jupiter–Io interaction. Tidal SPI, on the other hand, can naturally generate signals at harmonics of the orbital period, particularly at $P_{\text{orb}}/2$, owing to the formation of two tidal bulges on opposite hemispheres of the star (e.g. Cuntz et al., 2000). Consequently, searches for SPI signatures should account not only for the orbital and synodic periods, but also for their relevant harmonics.

In extreme close-in systems, tidal dissipation and magnetic torques may also lead to secular orbital evolution, causing the orbital period itself to vary with time. In such cases, SPI signatures are not expected to remain stable over long temporal baselines, but will instead show a gradual phase drift associated with orbital decay (e.g. Yee et al., 2020; Strugarek et al., 2017). This effect can broaden or shift peaks in classical periodograms and may require searches based on time-dependent ephemerides rather than a constant orbital period. Such behaviour is particularly relevant for ultra-short-period planets and systems undergoing strong tidal or magnetic dissipation.

Dataset splitting and rolling periodograms

One critical complication that distinguishes SPI searches from conventional period searches is the intermittent, or “on/off”, nature of the interaction itself. Observational evidence shows that SPI signals can appear and disappear across different epochs, possibly as a consequence of changes in the stellar magnetic topology over the activity cycle or variations in the coupling efficiency as the star’s large-scale magnetic field evolves (e.g. Shkolnik et al., 2008b; Lanza, 2012; Revilla et al., 2026). When the interaction is active during only a subset of the observations, combining all available data into a single set effectively dilutes the signal, thereby reducing its power in the periodogram.

One way to address this problem is to divide the full dataset into shorter, contiguous subsets, each spanning a single observing season or a well-defined temporal epoch, and analyse them independently (Shkolnik et al., 2003; Revilla et al., 2026). This approach mitigates signal dilution at the expense of a shorter temporal baseline and requires that each subset contain enough observations to resolve the periods of interest. The choice of subsets or timescales should also be guided by physical considerations and external information, as it directly impacts the detectability of potential signals.

An alternative strategy to factor in the evolving nature of SPI signals is to use rolling periodograms (Herbort, 2018; Schöfer, 2021). Rather than dividing the data into a fixed set of non-overlapping blocks, the rolling periodogram slides a window of a fixed size m of observations along the time series, computing a GLS periodogram for each window position. The collection of periodograms is then displayed as a two-dimensional map of power as a function of frequency and time, allowing to visualize the emergence, persistence, and decay of periodic signals across the observation record. The window length m represents a trade-off: too short a window fails to resolve closely spaced periods, while too long a window averages over transient behaviour. Rolling periodograms are particularly well suited to the study of SPI because they not only reveal whether a signal is present, but also identify the epochs during which the interaction is strongest, thereby guiding the selection of the most informative sub-datasets for detailed analysis.

False alarm probability and bootstrap significance

Assessing the statistical significance of a periodogram peak is therefore central to any detection claim. The standard metric is the False Alarm Probability (FAP), defined as the probability that a signal with the observed power, or greater, could arise purely from noise. Analytical estimates of the FAP are readily available for Lomb–Scargle-type periodograms (Baluev, 2008; Zechmeister and Kürster, 2009), but they rely on assumptions of Gaussian white noise and weakly correlated sampling that are rarely satisfied in practice. In SPI searches, additional complications arise from red noise associated with evolving stellar activity, irregular sampling, and the fact that the frequency of interest is often known a priori from the system ephemeris. In this latter case, the relevant question is not the probability of

finding a strong peak anywhere in the spectrum (the global FAP), but rather the probability of finding such a peak at a specific, predetermined frequency (the local FAP). Since the number of independent frequencies being tested is effectively unity, the local FAP can be orders of magnitude smaller than the global FAP, making it a substantially more informative quantity for assessing the significance of candidate SPI signals.

A robust approach for estimating the local FAP is bootstrap randomization combined with a frequency-windowing technique (Hatzes, 2019). The procedure consists of randomly shuffling the observed data values while keeping the observation timestamps fixed, thereby preserving the spectral window and the overall statistical properties of the original dataset. The GLS periodogram is then recomputed for a large number of realizations ($\sim 10^5$ – 10^6), and the fraction of cases in which the power within a narrow window centred on the frequency of interest exceeds the observed power provides the bootstrap FAP. Repeating the procedure with progressively narrower windows and extrapolating to zero width yields an empirical estimate of the probability that random noise alone could reproduce the observed signal at the exact frequency under consideration, rather than anywhere within a broader frequency interval. This approach is less sensitive to the assumed noise model than analytical estimates and is generally more robust against departures from ideal white-noise assumptions, including non-Gaussian statistics and weakly correlated residuals.

Taken together, these considerations illustrate that the detection of SPI signatures requires methodologies capable of accounting for complex stellar variability, irregular sampling, evolving signals, and prior knowledge of the characteristic interaction timescales. Robust identification therefore relies not on a single significant signal, but rather on the detection of a coherent physical pattern across time, consistent with the expected behaviour of star–planet interactions and, ideally, across multiple diagnostics. In this context, an ideal approach would involve a formalism capable of distinguishing between SPI-affected and SPI-unaffected measurements, thereby isolating the contribution of the interaction from the intrinsic variability of the host star.

Concluding remarks

The observational study of star–planet interactions (SPI) remains challenging, primarily because these signatures are often subtle, intermittent, and difficult to disentangle from intrinsic stellar variability. As discussed throughout this chapter, a wide range of diagnostics—including radial velocities, precision photometry, chromospheric activity indicators, radio observations, and transmission spectroscopy—provide complementary probes of SPI across different atmospheric layers and physical regimes. Robust identification requires consistent evidence across multiple observables, timescales, and analysis methods.

A central theme emerging from current studies is that stellar variability is not merely a source of noise, but a fundamental limitation that must be modeled carefully. Advances in time-series analysis, correlated-noise modeling, and statistical validation have significantly improved our ability to assess the significance of potential SPI signals. At the same time, geometry, stellar magnetic topology, and observational biases play a critical role in shaping the detectability and interpretation of these signals.

Radio observations, in particular, offer a unique and potentially direct probe of magnetic SPI through coherent emission mechanisms, with the ability to constrain planetary magnetic fields and magnetospheric interactions via polarization, spectral, and temporal diagnostics. Even non-detections in radio can place meaningful constraints on stellar wind properties and interaction regimes.

Transmission spectroscopy and chromospheric diagnostics provide particularly valuable insights into the coupling between stellar radiation, winds, and planetary atmospheres, while photometric techniques such as spot occultations offer spatially resolved information on stellar surfaces and potential orbit-locked activity. Nevertheless, stellar heterogeneity, especially starspots and faculae, remains a major

source of contamination, affecting both SPI diagnostics and atmospheric characterization.

Looking ahead, progress in this field will depend on combining multi-wavelength observations with physically motivated models that account for stellar magnetic structure and temporal variability. The synergy between current and upcoming facilities, including high-resolution spectrographs and space-based missions such as PLATO and HWO, will be essential to move from tentative detections toward a more systematic and physically grounded understanding of star–planet interactions.

Acknowledgements

Pedro Figueira thanks Pedro Amado for insightful comments on an early version of the manuscript.

PF, LPM, MPT, and DR acknowledge financial support from the Severo Ochoa grant CEX2021-001131-S funded by MCIN/AEI/10.13039/501100011033.

PF is funded by the European Union (ERC, THIRSTEE, 101164189). Views and opinions expressed are however those of the author(s) only and do not necessarily reflect those of the European Union or the European Research Council. Neither the European Union nor the granting authority can be held responsible for them.

LPM and MPT also acknowledge financial support from the Spanish grant PID2023-147883NB-C21, funded by MCIU/AEI/10.13039/501100011033, as well as support through ERDF/EU.

PC acknowledges the support of the Department of Atomic Energy, Government of India.

RF acknowledges support from the United Arab Emirates University (UAEU) UPAR grant number G00005451.

References

- Eva-Maria Ahrer, Michael Radica, Caroline Piaulet-Ghorayeb, Eshan Raul, Lindsey Wisser, Luis Welbanks, Lorena Acuña, Romain Allart, Louis-Philippe Coulombe, Amy Louca, Ryan MacDonald, Morgan Sidel, Thomas M. Evans-Soma, Björn Benneke, Duncan Christie, Thomas G. Beatty, Charles Cadieux, Ryan Cloutier, René Doyon, Jonathan J. Fortney, Anna Gagnebin, Cyril Gapp, Hamish Innes, Heather A. Knutson, Thaddeus Komacek, Joshua Krissansen-Totton, Yamila Miguel, Raymond Pierrehumbert, Pierre-Alexis Roy, and Hilke E. Schlichting. Escaping Helium and a Highly Muted Spectrum Suggest a Metal-enriched Atmosphere on Sub-Neptune GJ 3090 b from JWST Transit Spectroscopy. *ApJ*, 985(1):L10, May 2025. doi: 10.3847/2041-8213/add010.
- Suzanne Aigrain and Daniel Foreman-Mackey. Gaussian Process Regression for Astronomical Time Series. *ARA&A*, 61:329–371, August 2023. doi: 10.1146/annurev-astro-052920-103508.
- Vincenzo Andretta and Mark S. Giampapa. A Method for Estimating the Fractional Area Coverage of Active Regions on Dwarf F and G Stars. *ApJ*, 439:405, January 1995. doi: 10.1086/175183.
- Guillem Anglada-Escudé, Pedro J. Amado, John Barnes, Zaira M. Berdiñas, R. Paul Butler, Gavin A. L. Coleman, Ignacio de La Cueva, Stefan Dreizler, Michael Endl, Benjamin Giesers, Sandra V. Jeffers, James S. Jenkins, Hugh R. A. Jones, Marcin Kiraga, Martin Kürster, María J. López-González, Christopher J. Marvin, Nicolás Morales, Julien Morin, Richard P. Nelson, José L. Ortiz, Aviv Ofir, Sijme-Jan Paardekooper, Ansgar Reiners, Eloy Rodríguez, Cristina Rodríguez-López, Luis F. Sarmiento, John P. Strachan, Yiannis Tsapras, Mikko Tuomi, and Mathias Zechmeister. A terrestrial planet candidate in a temperate orbit around Proxima Centauri. *Nature*, 536(7617): 437–440, August 2016. doi: 10.1038/nature19106.
- Ruth Angus, Timothy Morton, Suzanne Aigrain, Daniel Foreman-Mackey, and Vinesh Rajpaul. Inferring probabilistic stellar rotation periods using Gaussian processes. *MNRAS*, 474(2):2094–2108, February 2018. doi: 10.1093/mnras/stx2109.

- Alexandre Araújo and Adriana Valio. Kepler-411 Differential Rotation from Three Transiting Planets. *ApJ*, 907(1):L5, January 2021. doi: 10.3847/2041-8213/abd3a7.
- Alexandre Araújo and Adriana Valio. The connection between starspots and superflares: a case study of two stars. *MNRAS*, 522(1):L16–L20, June 2023. doi: 10.1093/mnras/slاد034.
- Alexandre Araújo, Ciria Lima, Fabian Menezes, and Adriana Valio. Starspot Area Coverage: Correlation with Age and Spectral Type in FGK and M Stars. *ApJ*, 985(2):L28, June 2025. doi: 10.3847/2041-8213/add338.
- Étienne Artigau, Charles Cadieux, Neil J. Cook, René Doyon, Thomas Vandal, Jean-François Donati, Claire Moutou, Xavier Delfosse, Pascal Fouqué, Eder Martioli, François Bouchy, Jasmine Parsons, Andres Carmona, Xavier Dumusque, Nicola Astudillo-Defru, Xavier Bonfils, and Lucille Mignon. Line-by-line Velocity Measurements: an Outlier-resistant Method for Precision Velocimetry. *AJ*, 164(3):84, September 2022. doi: 10.3847/1538-3881/ac7ce6.
- R. V. Baluev. Assessing the statistical significance of periodogram peaks. *MNRAS*, 385(3):1279–1285, April 2008. doi: 10.1111/j.1365-2966.2008.12689.x.
- A. Baranne, D. Queloz, M. Mayor, G. Adrianzyk, G. Knispel, D. Kohler, D. Lacroix, J. P. Meunier, G. Rimbaud, and A. Vin. ELODIE: A spectrograph for accurate radial velocity measurements. *A&AS*, 119:373–390, October 1996.
- J. R. Barnes, S. V. Jeffers, C. A. Haswell, M. Damasso, F. Del Sordo, F. Liebing, M. Perger, and G. Anglada-Escudé. Identifying activity induced RV periodicities and correlations using central line moments. *MNRAS*, 534(2):1257–1282, October 2024. doi: 10.1093/mnras/stae2125.
- Lotfi Ben-Jaffel, Gilda E. Ballester, Antonio García Muñoz, Panayotis Lavvas, David K. Sing, Jorge Sanz-Forcada, Ofer Cohen, Tiffany Kataria, Gregory W. Henry, Lars Buchhave, Thomas Mikal-Evans, Hannah R. Wakeford, and Mercedes López-Morales. Signatures of strong magnetization and a metal-poor atmosphere for a Neptune-sized exoplanet. *Nature Astronomy*, 6:141–153, January 2022. doi: 10.1038/s41550-021-01505-x.
- Svetlana V. Berdyugina. Starspots: A Key to the Stellar Dynamo. *Living Reviews in Solar Physics*, 2(1):8, December 2005. doi: 10.12942/lrsp-2005-8.
- I. Boisse, F. Bouchy, G. Hébrard, X. Bonfils, N. Santos, and S. Vauclair. Disentangling between stellar activity and planetary signals. *A&A*, 528:A4, April 2011. doi: 10.1051/0004-6361/201014354.
- F. Bouchy, F. Pepe, and D. Queloz. Fundamental photon noise limit to radial velocity measurements. *A&A*, 374:733–739, August 2001. doi: 10.1051/0004-6361:20010730.
- V. Bourrier, A. Lecavelier des Etangs, D. Ehrenreich, J. Sanz-Forcada, R. Allart, G. E. Ballester, L. A. Buchhave, O. Cohen, D. Deming, T. M. Evans, A. García Muñoz, G. W. Henry, T. Kataria, P. Lavvas, N. Lewis, M. López-Morales, M. Marley, D. K. Sing, and H. R. Wakeford. Hubble PanCET: an extended upper atmosphere of neutral hydrogen around the warm Neptune GJ 3470b. *A&A*, 620:A147, December 2018. doi: 10.1051/0004-6361/201833675.
- J. R. Callingham, H. K. Vedantham, T. W. Shimwell, B. J. S. Pope, I. E. Davis, P. N. Best, M. J. Hardcastle, H. J. A. Röttgering, J. Sabater, C. Tasse, R. J. van Weeren, W. L. Williams, P. Zarka, F. de Gasperin, and A. Drabent. The population of M dwarfs observed at low radio frequencies. *Nature Astronomy*, 5:1233–1239, December 2021. doi: 10.1038/s41550-021-01483-0.
- J. R. Callingham, B. J. S. Pope, R. D. Kavanagh, S. Bellotti, S. Daley-Yates, M. Damasso, J.-M. Grießmeier, M. Güdel, M. Günther, M. M. Kao, B. Klein, S. Mahadevan, J. Morin, J. D. Nichols, R. A. Osten, M. Pérez-Torres, J. S. Pineda, J. Rigney, J. Saur, G. Stefánsson, J. D. Turner, H. Vedantham, A. A. Vidotto, J. Villadsen, and P. Zarka. Radio signatures of star-planet interactions, exoplanets and space weather. *Nature Astronomy*, 8:1359–1372, November 2024. doi: 10.1038/s41550-024-02405-6.

- P. Wilson Cauley, Evgenya L. Shkolnik, Joe Llama, Vincent Bourrier, and Claire Moutou. Evidence of Magnetic Star-Planet Interactions in the HD 189733 System from Orbitally Phased Ca II K Variations. *AJ*, 156(6):262, December 2018. doi: 10.3847/1538-3881/aae841.
- P. Wilson Cauley, Evgenya L. Shkolnik, Ilya Ilyin, Klaus G. Strassmeier, Seth Redfield, and Adam Jensen. Atmospheric Dynamics and the Variable Transit of KELT-9 b. *AJ*, 157(2):69, February 2019. doi: 10.3847/1538-3881/aaf725.
- C. Cecchi-Pestellini, A. Ciaravella, and G. Micela. Stellar X-ray heating of planet atmospheres. *A&A*, 458(2):L13–L16, November 2006. doi: 10.1051/0004-6361/20066093.
- A. Chelli. Optimizing Doppler estimates for extrasolar planet detection. I. A specific algorithm for shifted spectra. *A&A*, 358:L59–L62, June 2000.
- A. Cherenkov, D. Bisikalo, L. Fossati, and C. Möstl. The Influence of Coronal Mass Ejections on the Mass-loss Rates of Hot-Jupiters. *ApJ*, 846(1):31, September 2017. doi: 10.3847/1538-4357/aa82b2.
- Jessie L. Christiansen, Bruce D. Clarke, Christopher J. Burke, Jon M. Jenkins, Stephen T. Bryson, Jeffrey L. Coughlin, Fergal Mullally, Susan E. Thompson, Joseph D. Twicken, Natalie M. Batalha, Michael R. Haas, Joseph Catanzarite, Jennifer R. Campbell, AKM Kamal Uddin, Khadeejah Zamudio, Jeffrey C. Smith, and Christopher E. Henze. Measuring Transit Signal Recovery in the Kepler Pipeline. III. Completeness of the Q1-Q17 DR24 Planet Candidate Catalogue with Important Caveats for Occurrence Rate Calculations. *ApJ*, 828(2):99, September 2016. doi: 10.3847/0004-637X/828/2/99.
- C. Cincunegui, R. F. Díaz, and P. J. D. Mauas. $H\alpha$ and the Ca II H and K lines as activity proxies for late-type stars. *A&A*, 469(1):309–317, July 2007. doi: 10.1051/0004-6361/20066503.
- A. Collier Cameron, E. B. Ford, S. Shahaf, S. Aigrain, X. Dumusque, R. D. Haywood, A. Mortier, D. F. Phillips, L. Buchhave, M. Ceconi, H. Cegla, R. Cosentino, M. Crétignier, A. Ghedina, M. González, D. W. Latham, M. Lodi, M. López-Morales, G. Micela, E. Molinari, F. Pepe, G. Piotto, E. Poretti, D. Queloz, J. San Juan, D. Ségransan, A. Sozzetti, A. Szentgyorgyi, S. Thompson, S. Udry, and C. Watson. Separating planetary reflex Doppler shifts from stellar variability in the wavelength domain. *MNRAS*, 505(2):1699–1717, August 2021. doi: 10.1093/mnras/stab1323.
- M. Cretignier, X. Dumusque, R. Allart, F. Pepe, and C. Lovis. Measuring precise radial velocities on individual spectral lines. II. Dependence of stellar activity signal on line depth. *A&A*, 633:A76, January 2020. doi: 10.1051/0004-6361/201936548.
- Patricio Cubillos, Joseph Harrington, Thomas J. Loredo, Nate B. Lust, Jasmina Blečić, and Madison Stemm. On Correlated-noise Analyses Applied to Exoplanet Light Curves. *AJ*, 153(1):3, January 2017. doi: 10.3847/1538-3881/153/1/3.
- Patricio E. Cubillos, Matteo Brogi, Antonio García Muñoz, Luca Fossati, Sudeshna Boro Saikia, Vincent Bourrier, Jose A. Caballero, Juan Cabrera, Andrea Chiavassa, Andrzej Fludra, Leonardos Gkouvelis, John Lee Grenfell, Manuel Guedel, Alvaro Labiano, Monika Lendl, Donna Rodgers-Lee, Arnaud Salvador, Ilane Schroetter, Antoine Strugarek, Benjamin Taysum, Aline Vidotto, and Thomas G. Wilson. High-resolution Ultraviolet-to-nearinfrared Characterization of Exoplanet Atmospheres. *arXiv e-prints*, art. arXiv:2507.03060, July 2025. doi: 10.48550/arXiv.2507.03060.
- Manfred Cuntz, Steven H. Saar, and Zdzisław E. Musielak. On Stellar Activity Enhancement Due to Interactions with Extrasolar Giant Planets. *ApJ*, 533(2):L151–L154, April 2000. doi: 10.1086/312609.
- S. Czesla, M. Lampón, J. Sanz-Forcada, A. García Muñoz, M. López-Puertas, L. Nortmann, D. Yan, E. Nagel, F. Yan, J. H. M. M. Schmitt, J. Aceituno, P. J. Amado, J. A. Caballero, N. Casasayas-Barris, Th. Henning, S. Khalafinejad, K. Molaverdikhani, D. Montes, E. Pallé, A. Reiners, P. C. Schneider, I. Ribas, A. Quirrenbach, M. R. Zapatero Osorio, and M. Zechmeister. $H\alpha$ and He I absorption in HAT-P-32 b observed with CARMENES. Detection of Roche lobe overflow and mass loss. *A&A*, 657:A6, January 2022. doi: 10.1051/0004-6361/202039919.

- James R. A. Davenport. The Kepler Catalog of Stellar Flares. *ApJ*, 829(1):23, September 2016. doi: 10.3847/0004-637X/829/1/23.
- Conaire Deagan and Benjamin T. Montet. Inferring hemispheric asymmetries of stellar active regions through the information content of astrometric signals. *arXiv e-prints*, art. arXiv:2601.11707, January 2026. doi: 10.48550/arXiv.2601.11707.
- Rodrigo F. Díaz, Carolina Cincunegui, and Pablo J. D. Mauas. The NaI D resonance lines in main-sequence late-type stars. *MNRAS*, 378(3):1007–1018, July 2007. doi: 10.1111/j.1365-2966.2007.11833.x.
- Leonardo A. Dos Santos, Eric D. Lopez, Luca Fossati, Antonio García Muñoz, Shingo Kameda, Munazza K. Alam, Keighley Rockcliffe, Seth Redfield, Yuichi Ito, Joshua Lothringer, Shreyas Vissapragada, Hannah R. Wakeford, Apurva V. Oza, Girish M. Duvvuri, Raissa Estrela, Ryoya Sakata, Chuanfei Dong, and Ziyu Huang. Exoplanet Atmospheric Escape Observations with the Habitable Worlds Observatory. *arXiv e-prints*, art. arXiv:2507.07124, July 2025. doi: 10.48550/arXiv.2507.07124.
- X. Dumusque. Measuring precise radial velocities on individual spectral lines. I. Validation of the method and application to mitigate stellar activity. *A&A*, 620:A47, November 2018. doi: 10.1051/0004-6361/201833795.
- A. Duquennoy and M. Mayor. Multiplicity among Solar Type Stars in the Solar Neighbourhood - Part Two - Distribution of the Orbital Elements in an Unbiased Sample. *A&A*, 248:485, August 1991.
- R. Fares, J.-F. Donati, C. Moutou, D. Bohlender, C. Catala, M. Deleuil, E. Shkolnik, A. Collier Cameron, M. M. Jardine, and G. A. H. Walker. Magnetic cycles of the planet-hosting star τ Bootis - II. A second magnetic polarity reversal. *MNRAS*, 398(3):1383–1391, September 2009. doi: 10.1111/j.1365-2966.2009.15303.x.
- R. Fares, J.-F. Donati, C. Moutou, M. M. Jardine, J.-M. Grießmeier, P. Zarka, E. L. Shkolnik, D. Bohlender, C. Catala, and A. Collier Cameron. Searching for star-planet interactions within the magnetosphere of HD189733. *MNRAS*, 406(1):409–419, July 2010. doi: 10.1111/j.1365-2966.2010.16715.x.
- R. Fares, J.-F. Donati, C. Moutou, M. Jardine, A. C. Cameron, A. F. Lanza, D. Bohlender, S. Dieters, A. F. Martínez Fiorenzano, A. Maggio, I. Pagano, and E. L. Shkolnik. Magnetic field, differential rotation and activity of the hot-Jupiter-hosting star HD 179949. *MNRAS*, 423(2):1006–1017, June 2012. doi: 10.1111/j.1365-2966.2012.20780.x.
- J. P. Faria, A. Suárez Mascareño, P. Figueira, A. M. Silva, M. Damasso, O. Demangeon, F. Pepe, N. C. Santos, R. Rebolo, S. Cristiani, V. Adibekyan, Y. Alibert, R. Allart, S. C. C. Barros, A. Cabral, V. D’Odorico, P. Di Marcantonio, X. Dumusque, D. Ehrenreich, J. I. González Hernández, N. Hara, J. Lillo-Box, G. Lo Curto, C. Lovis, C. J. A. P. Martins, D. Mégevand, A. Mehner, G. Micela, P. Molaro, N. J. Nunes, E. Pallé, E. Poretti, S. G. Sousa, A. Sozzetti, H. Tabernero, S. Udry, and M. R. Zapatero Osorio. A candidate short-period sub-Earth orbiting Proxima Centauri. *A&A*, 658:A115, February 2022. doi: 10.1051/0004-6361/202142337.
- Adina D. Feinstein, Benjamin T. Montet, Megan Ansdell, Brian Nord, Jacob L. Bean, Maximilian N. Günther, Michael A. Gully-Santiago, and Joshua E. Schlieder. Flare Statistics for Young Stars from a Convolutional Neural Network Analysis of TESS Data. *AJ*, 160(5):219, November 2020. doi: 10.3847/1538-3881/abac0a.
- P. Figueira, N. C. Santos, F. Pepe, C. Lovis, and N. Nardetto. Line-profile variations in radial-velocity measurements. Two alternative indicators for planetary searches. *A&A*, 557:A93, September 2013. doi: 10.1051/0004-6361/201220779.
- P. Figueira, J. P. Faria, A. M. Silva, A. Castro-González, J. Gomes da Silva, S. G. Sousa, D. Bossini, M. R. Zapatero-Osorio, O. Balsalobre-Ruza, J. Lillo-Box, H. M. Tabernero, V. Adibekyan, R. Allart, S. Benatti, F. Bouchy, A. Cabral, S. Cristiani, X. Dumusque, J. I. González-Hernández, N. Hara, G. Lo Curto, C. Lovis, A. Mehner, P. Molaro, F. Pepe, N. C. Santos, D. Ségransan, D. Sosnowska,

- R. Rebolo, A. Suárez Mascareño, A. Sozzetti, S. Udry, and B. Wehbe. A comprehensive study on radial velocity signals using ESPRESSO: Pushing precision to the 10 cm/s level. *A&A*, 700:A174, August 2025. doi: 10.1051/0004-6361/202553869.
- Pedro Figueira. Deriving High-Precision Radial Velocities. In Tiago L. Campante, Nuno C. Santos, and Mário J. P. F. G. Monteiro, editors, *Asteroseismology and Exoplanets: Listening to the Stars and Searching for New Worlds*, volume 49 of *Astrophysics and Space Science Proceedings*, page 181, January 2018. doi: 10.1007/978-3-319-59315-9_10.
- Christian Fischer and Joachim Saur. Time-variable electromagnetic star–planet interaction: The TRAPPIST-1 system as an exemplary case. *ApJ*, 872(1):113, February 2019. ISSN 1538-4357. doi: 10.3847/1538-4357/aafaf2.
- Daniel Foreman-Mackey, Eric Agol, Sivaram Ambikasaran, and Ruth Angus. Fast and Scalable Gaussian Process Modeling with Applications to Astronomical Time Series. *AJ*, 154(6):220, December 2017. doi: 10.3847/1538-3881/aa9332.
- B. Fuhrmeister, S. Czesla, J. H. M. M. Schmitt, E. N. Johnson, P. Schöfer, S. V. Jeffers, J. A. Caballero, M. Zechmeister, A. Reiners, I. Ribas, P. J. Amado, A. Quirrenbach, F. Bauer, V. J. S. Béjar, M. Cortés-Contreras, E. Díez Alonso, S. Dreizler, D. Galadí-Enríquez, E. W. Guenther, A. Kaminski, M. Kürster, M. Lafarga, and D. Montes. The CARMENES search for exoplanets around M dwarfs. Period search in H α , Na I D, and Ca II IRT lines. *A&A*, 623:A24, March 2019. doi: 10.1051/0004-6361/201834483.
- F. Galland, A. M. Lagrange, S. Udry, A. Chelli, F. Pepe, D. Queloz, J. L. Beuzit, and M. Mayor. Extrasolar planets and brown dwarfs around A-F type stars. I. Performances of radial velocity measurements, first analyses of variations. *A&A*, 443(1):337–345, November 2005. doi: 10.1051/0004-6361:20052938.
- A. García Muñoz. Physical and chemical aeronomy of HD 209458b. *Planet. Space Sci.*, 55(10):1426–1455, July 2007. doi: 10.1016/j.pss.2007.03.007.
- A. García Muñoz. Heating and ionization by non-thermal electrons in the upper atmospheres of water-rich exoplanets. *A&A*, 672:A77, April 2023. doi: 10.1051/0004-6361/202245766.
- A. García Muñoz. Modeling helium in exoplanet atmospheres. A revised network with photoelectron-driven processes. *A&A*, 698:A199, June 2025. doi: 10.1051/0004-6361/202555145.
- A. García Muñoz and P. C. Schneider. Rapid Escape of Ultra-hot Exoplanet Atmospheres Driven by Hydrogen Balmer Absorption. *ApJ*, 884(2):L43, October 2019. doi: 10.3847/2041-8213/ab498d.
- A. García Muñoz, A. Youngblood, L. Fossati, D. Gandolfi, J. Cabrera, and H. Rauer. Is π Men c’s Atmosphere Hydrogen-dominated? Insights from a Non-detection of H I Ly α Absorption. *ApJ*, 888(2):L21, January 2020. doi: 10.3847/2041-8213/ab61ff.
- A. García Muñoz, L. Fossati, A. Youngblood, N. Nettelmann, D. Gandolfi, J. Cabrera, and H. Rauer. A Heavy Molecular Weight Atmosphere for the Super-Earth π Men c. *ApJ*, 907(2):L36, February 2021. doi: 10.3847/2041-8213/abd9b8.
- A. García Muñoz, D. De Fazio, D. J. Wilson, and K. France. Vibrationally excited H₂ muting the He I triplet line at 1.08 μ m on warm exo-Neptunes. *A&A*, 704:L18, December 2025. doi: 10.1051/0004-6361/202558117.
- A. Gillet, A. Strugarek, and A. García Muñoz. Secondary ionisation in hot atmospheres and interactions between planetary and stellar winds. *A&A*, 696:A64, April 2025. doi: 10.1051/0004-6361/202452559.
- J. Gomes da Silva, N. C. Santos, X. Bonfils, X. Delfosse, T. Forveille, and S. Udry. Long-term magnetic activity of a sample of M-dwarf stars from the HARPS program. I. Comparison of activity indices. *A&A*, 534:A30, October 2011. doi: 10.1051/0004-6361/201116971.

- J. Gomes da Silva, A. Bensabat, T. Monteiro, and N. C. Santos. Optimising the H α index for the identification of activity signals in FGK stars. Improvement of the correlation between H α and Ca II H&K. *A&A*, 668:A174, December 2022. doi: 10.1051/0004-6361/202244595.
- Ana I. Gómez de Castro, Martin A. Barstow, Frederic Baudin, Stefano Benetti, Jean Claude Bouret, Noah Brosch, Ada Canet, Domitilla de Martino, Giulio Del Zanna, Chris Evans, Kevin France, Miriam García, Boris Gaensicke, Lynne Hillenbrand, Eric Josselin, Carolina Kehrig, Laurent Lamy, Jon Lapington, Alain Lecavelier des Etangs, Giampiero Naletto, Yael Nazé, Coralie Neiner, Jonathan Nichols, Marina Orio, Isabella Pagano, Céline Peroux, Gregor Rauw, Steven Shore, Gagik Tovmasian, and Asif ud-Doula. Closing gaps to our origins. *Experimental Astronomy*, 54(2-3):1307–1337, December 2022. doi: 10.1007/s10686-022-09854-9.
- David F. Gray. Shapes of Spectral Line Bisectors for Cool Stars. *PASP*, 117(833):711–720, July 2005a. doi: 10.1086/430412.
- David F. Gray. *The Observation and Analysis of Stellar Photospheres*. 2005b. doi: 10.1017/CBO9781316036570.
- G. Guilluy, V. Andretta, F. Borsa, P. Giacobbe, A. Sozzetti, E. Covino, V. Bourrier, L. Fossati, A. S. Bonomo, M. Esposito, M. S. Giampapa, A. Harutyunyan, M. Rainer, M. Brogi, G. Bruno, R. Claudi, G. Frustagli, A. F. Lanza, L. Mancini, L. Pino, E. Poretti, G. Scandariato, L. Affer, C. Baffa, A. Baruffolo, S. Benatti, K. Biazzo, A. Bignamini, W. Boschin, I. Carleo, M. Ceconi, R. Cosentino, M. Damasso, S. Desidera, G. Falcini, A. F. Martinez Fiorenzano, A. Ghedina, E. González-Álvarez, J. Guerra, N. Hernandez, G. Leto, A. Maggio, L. Malavolta, J. Maldonado, G. Micela, E. Molinari, V. Nascimbeni, I. Pagano, M. Pedani, G. Piotto, and A. Reiners. The GAPS programme at TNG. XXII. The GIARPS view of the extended helium atmosphere of HD 189733 b accounting for stellar activity. *A&A*, 639:A49, July 2020. doi: 10.1051/0004-6361/202037644.
- G. Guilluy, M. C. D’Arpa, A. S. Bonomo, R. Spinelli, F. Biassoni, L. Fossati, A. Maggio, P. Giacobbe, A. F. Lanza, A. Sozzetti, F. Borsa, M. Rainer, G. Micela, L. Affer, G. Andreuzzi, A. Bignamini, W. Boschin, I. Carleo, M. Ceconi, S. Desidera, V. Fardella, A. Ghedina, G. Mantovan, L. Mancini, V. Nascimbeni, C. Knapic, M. Pedani, A. Petralia, L. Pino, G. Scandariato, D. Sicilia, M. Stangret, and T. Zingales. The GAPS Programme at TNG. LIV. A He I survey of close-in giant planets hosted by M-K dwarf stars with GIANO-B. *A&A*, 686:A83, June 2024. doi: 10.1051/0004-6361/202348997.
- Jeffrey C. Hall. Stellar Chromospheric Activity. *Living Reviews in Solar Physics*, 5(1):2, December 2008. doi: 10.12942/lrsp-2008-2.
- A. P. Hatzes. *The Doppler Method for the Detection of Exoplanets*. IOP Publishing, 2019. ISBN 978-0-7503-1689-7. doi: 10.1088/2514-3433/ab46a3.
- Gopal Hazra, Aline A. Vidotto, Stephen Carolan, Carolina Villarreal D’Angelo, and Ward Manchester. The impact of coronal mass ejections and flares on the atmosphere of the hot Jupiter HD189733b. *MNRAS*, 509(4):5858–5871, February 2022. doi: 10.1093/mnras/stab3271.
- Oliver Herbort. Stellar activity in cn leo. Master’s thesis, Institut für Astrophysik Göttingen, Göttingen, Germany, August 2018. <https://carnenes.caha.es/int/documents/theses/msc.uni-goe.herbort.pdf>.
- Michael Hippke, Trevor J. David, Gijs D. Mulders, and René Heller. Wotan: Comprehensive Time-series Detrending in Python. *AJ*, 158(4):143, October 2019. doi: 10.3847/1538-3881/ab3984.
- Daniel Huber. The Space-Based Time-Domain Revolution in Astrophysics. *arXiv e-prints*, art. arXiv:2512.10002, December 2025. doi: 10.48550/arXiv.2512.10002.
- N. Huélamo, P. Figueira, X. Bonfils, N. C. Santos, F. Pepe, M. Gillon, R. Azevedo, T. Barman, M. Fernández, E. di Folco, E. W. Guenther, C. Lovis, C. H. F. Melo, D. Queloz, and S. Udry. TW Hydrae: evidence of stellar spots instead of a Hot Jupiter. *A&A*, 489(2):L9–L13, October 2008. doi: 10.1051/0004-6361:200810596.

- R. V. Ibañez Bustos, A. P. Buccino, M. Flores, C. F. Martinez, and P. J. D. Mauas. Correlation between activity indicators: H α and Ca II lines in M-dwarf stars. *A&A*, 672:A37, April 2023. doi: 10.1051/0004-6361/202245352.
- Ekaterina Ilin, Katja Poppenhäger, Judy Chebly, Nikoleta Ilić, and Julián D. Alvarado-Gómez. Planetary perturbers: flaring star-planet interactions in Kepler and TESS. *MNRAS*, 527(2):3395–3417, January 2024. doi: 10.1093/mnras/stad3398.
- Ekaterina Ilin, Harish K. Vedantham, Katja Poppenhäger, Sanne Bloot, Joseph R. Callingham, Alexis Brandeker, and Hritam Chakraborty. Close-in planet induces flares on its host star. *Nature*, 643(8072):645–648, July 2025. doi: 10.1038/s41586-025-09236-z.
- James S. Jenkins, Joseph Harrington, Ryan C. Challener, Nicolás T. Kurtovic, Ricardo Ramirez, Jose Peña, Kathleen J. McIntyre, Michael D. Himes, Eloy Rodríguez, Guillem Anglada-Escudé, Stefan Dreizler, Aviv Ofir, Pablo A. Peña Rojas, Ignasi Ribas, Patricio Rojo, David Kipping, R. Paul Butler, Pedro J. Amado, Cristina Rodríguez-López, Eliza M.-R. Kempton, Enric Palle, and Felipe Murgas. Proxima Centauri b is not a transiting exoplanet. *MNRAS*, 487(1):268–274, July 2019. doi: 10.1093/mnras/stz1268.
- M. L. Khodachenko, I. F. Shaikhislamov, H. Lammer, A. G. Berezutsky, I. B. Miroshnichenko, M. S. Rumenskikh, K. G. Kislyakova, and N. K. Dwivedi. Global 3D Hydrodynamic Modeling of In-transit Ly α Absorption of GJ 436b. *ApJ*, 885(1):67, November 2019. doi: 10.3847/1538-4357/ab46a4.
- M. L. Khodachenko, I. F. Shaikhislamov, H. Lammer, I. B. Miroshnichenko, M. S. Rumenskikh, A. G. Berezutsky, and L. Fossati. The impact of intrinsic magnetic field on the absorption signatures of elements probing the upper atmosphere of HD209458b. *MNRAS*, 507(3):3626–3637, November 2021. doi: 10.1093/mnras/stab2366.
- Baptiste Klein, Norbert Zicher, Robert D. Kavanagh, Louise D. Nielsen, Suzanne Aigrain, Aline A. Vidotto, Oscar Barragán, Antoine Strugarek, Belinda Nicholson, Jean-François Donati, and Jérôme Bouvier. One year of AU Mic with HARPS - II. Stellar activity and star-planet interaction. *MNRAS*, 512(4):5067–5084, June 2022. doi: 10.1093/mnras/stac761.
- Jennifer R. Kulow, Kevin France, Jeffery Linsky, and R. O. Parke Loyd. Ly α Transit Spectroscopy and the Neutral Hydrogen Tail of the Hot Neptune GJ 436b. *ApJ*, 786(2):132, May 2014. doi: 10.1088/0004-637X/786/2/132.
- D. Kuridze, M. Mathioudakis, P. J. A. Simões, L. Rouppe van der Voort, M. Carlsson, S. Jafarzadeh, J. C. Allred, A. F. Kowalski, M. Kennedy, L. Fletcher, D. Graham, and F. P. Keenan. H α Line Profile Asymmetries and the Chromospheric Flare Velocity Field. *ApJ*, 813(2):125, November 2015. doi: 10.1088/0004-637X/813/2/125.
- M. Kürster, M. Endl, F. Rouesnel, S. Els, A. Kaufer, S. Brilliant, A. P. Hatzes, S. H. Saar, and W. D. Cochran. The low-level radial velocity variability in Barnard’s star (= GJ 699). Secular acceleration, indications for convective redshift, and planet mass limits. *A&A*, 403:1077–1087, June 2003. doi: 10.1051/0004-6361:20030396.
- M. Lafarga, I. Ribas, C. Lovis, M. Perger, M. Zechmeister, F. F. Bauer, M. Kürster, M. Cortés-Contreras, J. C. Morales, E. Herrero, A. Rosich, D. Baroch, A. Reiners, J. A. Caballero, A. Quirrenbach, P. J. Amado, J. M. Alacid, V. J. S. Béjar, S. Dreizler, A. P. Hatzes, T. Henning, S. V. Jeffers, A. Kaminski, D. Montes, S. Pedraz, C. Rodríguez-López, and J. H. M. M. Schmitt. The CARMENES search for exoplanets around M dwarfs. Radial velocities and activity indicators from cross-correlation functions with weighted binary masks. *A&A*, 636:A36, April 2020. doi: 10.1051/0004-6361/201937222.
- A. F. Lanza. Hot Jupiters and stellar magnetic activity. *A&A*, 487(3):1163–1170, September 2008. doi: 10.1051/0004-6361:200809753.
- A. F. Lanza. Star-planet magnetic interaction and activity in late-type stars with close-in planets. *A&A*, 544:A23, August 2012. doi: 10.1051/0004-6361/201219002.

- A. F. Lanza, I. Pagano, G. Leto, S. Messina, S. Aigrain, R. Alonso, M. Auvergne, A. Baglin, P. Barge, A. S. Bonomo, P. Boumier, A. Collier Cameron, M. Comparato, G. Cutispoto, J. R. de Medeiros, B. Foing, A. Kaiser, C. Moutou, P. S. Parihar, A. Silva-Valio, and W. W. Weiss. Magnetic activity in the photosphere of CoRoT-Exo-2a. Active longitudes and short-term spot cycle in a young Sun-like star. *A&A*, 493(1):193–200, January 2009. doi: 10.1051/0004-6361/200810591.
- B. Lavie, D. Ehrenreich, V. Bourrier, A. Lecavelier des Etangs, A. Vidal-Madjar, X. Delfosse, A. Gracia Berna, K. Heng, N. Thomas, S. Udry, and P. J. Wheatley. The long egress of GJ 436b’s giant exosphere. *A&A*, 605:L7, September 2017. doi: 10.1051/0004-6361/201731340.
- A. Lecavelier Des Etangs, D. Ehrenreich, A. Vidal-Madjar, G. E. Ballester, J.-M. Désert, R. Ferlet, G. Hébrard, D. K. Sing, K.-O. Tchakoumegni, and S. Udry. Evaporation of the planet HD 189733b observed in H I Lyman- α . *A&A*, 514:A72, May 2010. doi: 10.1051/0004-6361/200913347.
- A. Lecavelier des Etangs, V. Bourrier, P. J. Wheatley, H. Dupuy, D. Ehrenreich, A. Vidal-Madjar, G. Hébrard, G. E. Ballester, J.-M. Désert, R. Ferlet, and D. K. Sing. Temporal variations in the evaporating atmosphere of the exoplanet HD 189733b. *A&A*, 543:L4, July 2012. doi: 10.1051/0004-6361/201219363.
- Jeffrey L. Linsky. Stellar Model Chromospheres and Spectroscopic Diagnostics. *ARA&A*, 55(1):159–211, August 2017. doi: 10.1146/annurev-astro-091916-055327.
- Jeffrey L. Linsky, Hao Yang, Kevin France, Cynthia S. Froning, James C. Green, John T. Stocke, and Steven N. Osterman. Observations of Mass Loss from the Transiting Exoplanet HD 209458b. *ApJ*, 717(2):1291–1299, July 2010. doi: 10.1088/0004-637X/717/2/1291.
- N. R. Lomb. Least-Squares Frequency Analysis of Unequally Spaced Data. *Ap&SS*, 39(2):447–462, February 1976. doi: 10.1007/BF00648343.
- C. Lovis, X. Dumusque, N. C. Santos, F. Bouchy, M. Mayor, F. Pepe, D. Queloz, D. Ségransan, and S. Udry. The HARPS search for southern extra-solar planets. XXXI. Magnetic activity cycles in solar-type stars: statistics and impact on precise radial velocities. *arXiv e-prints*, art. arXiv:1107.5325, July 2011. doi: 10.48550/arXiv.1107.5325.
- R. O. Parke Loyd, P. C. Schneider, James A. G. Jackman, Kevin France, Evgenya L. Shkolnik, Nicole Arulanantham, P. Wilson Cauley, Joe Llama, and Adam C. Schneider. Flares, Rotation, Activity Cycles, and a Magnetic Star–Planet Interaction Hypothesis for the Far-ultraviolet Emission of GJ 436. *AJ*, 165(4):146, April 2023. doi: 10.3847/1538-3881/acbbc8.
- R. O. Parke Loyd, Ethan Schreyer, James E. Owen, James G. Rogers, Madelyn I. Broome, Evgenya L. Shkolnik, Ruth Murray-Clay, David J. Wilson, Sarah Peacock, Johanna Teske, Hilke E. Schlichting, Girish M. Duvvuri, Allison Youngblood, P. Christian Schneider, Kevin France, Steven Giacalone, Natasha E. Batalha, Adam C. Schneider, Isabella Longo, Travis Barman, and David R. Ardila. Hydrogen escaping from a pair of exoplanets smaller than Neptune. *Nature*, 638(8051):636–639, February 2025. doi: 10.1038/s41586-024-08490-x.
- Rodrigo Luger, Daniel Foreman-Mackey, Christina Hedges, and David W. Hogg. Mapping Stellar Surfaces. I. Degeneracies in the Rotational Light-curve Problem. *AJ*, 162(3):123, September 2021. doi: 10.3847/1538-3881/abfdb8.
- C. San Nicolas Martinez, N. C. Santos, V. Adibekyan, K. Al Moulla, A. M. Silva, and S. G. Sousa. TILARA: Template-Independent Line-by-line Algorithm for Radial velocity Analysis. I. Description of the code and application on a Sun-like star. *arXiv e-prints*, art. arXiv:2603.05445, March 2026. doi: 10.48550/arXiv.2603.05445.
- A. Masson, S. Vinatier, B. Bézard, M. López-Puertas, M. Lampón, F. Debras, A. Carmona, B. Klein, E. Artigau, W. Dethier, S. Pelletier, T. Hood, R. Allart, V. Bourrier, C. Cadieux, B. Charnay, N. B. Cowan, N. J. Cook, X. Delfosse, J.-F. Donati, P.-G. Gu, G. Hébrard, E. Martioli, C. Moutou, O. Venot, and A. Wyttenbach. Probing atmospheric escape through metastable He I triplet lines in 15 exoplanets observed with SPIRou. *A&A*, 688:A179, August 2024. doi: 10.1051/0004-6361/202449608.

- Michel Mayor and Didier Queloz. A Jupiter-mass companion to a solar-type star. *Nature*, 378(6555): 355–359, November 1995. doi: 10.1038/378355a0.
- Tsevi Mazeh, Hagai B. Perets, Amy McQuillan, and Eyal S. Goldstein. Photometric Amplitude Distribution of Stellar Rotation of KOIs—Indication for Spin-Orbit Alignment of Cool Stars and High Obliquity for Hot Stars. *ApJ*, 801(1):3, March 2015. doi: 10.1088/0004-637X/801/1/3.
- A. McQuillan, S. Aigrain, and S. Roberts. Statistics of stellar variability from Kepler. I. Revisiting Quarter 1 with an astrophysically robust systematics correction. *A&A*, 539:A137, March 2012. doi: 10.1051/0004-6361/201016148.
- Fabian Menezes, Alexandre Araújo, and Adriana Valio. Probing the magnetic fields of starspots with transit mapping. *A&A*, 691:L12, November 2024. doi: 10.1051/0004-6361/202452071.
- N. Meunier, M. Kretzschmar, R. Gravet, L. Mignon, and X Delfosse. Relationship between Ca and H α chromospheric emission in F-G-K stars: indication of stellar filaments? *arXiv e-prints*, art. arXiv:2201.05492, January 2022.
- N. Meunier, L. Mignon, M. Kretzschmar, and X. Delfosse. Characterisation of the stellar activity of M dwarfs. II. Relationship between Ca, H α , and Na chromospheric emissions. *A&A*, 684:A106, April 2024. doi: 10.1051/0004-6361/202347362.
- Brendan P. Miller, Elena Gallo, Jason T. Wright, and Andrea K. Dupree. On the Detectability of Star-Planet Interaction. *ApJ*, 754(2):137, August 2012. doi: 10.1088/0004-637X/754/2/137.
- D. Montes, M. J. Fernandez-Figueroa, E. de Castro, and J. Sanz-Forcada. Multiwavelength optical observations of chromospherically active binary systems. I. Simultaneous H α , NA I D₁, D₂, and He I D₃ observations. *A&AS*, 125:263–287, October 1997. doi: 10.1051/aas:1997374.
- G. Morello. A Blind Method to Detrend Instrumental Systematics in Exoplanetary Light Curves. *ApJ*, 808(1):56, July 2015. doi: 10.1088/0004-637X/808/1/56.
- Brett M. Morris, Leslie Hebb, James R. A. Davenport, Graeme Rohn, and Suzanne L. Hawley. The Starspots of HAT-P-11: Evidence for a Solar-like Dynamo. *ApJ*, 846(2):99, September 2017. doi: 10.3847/1538-4357/aa8555.
- Kosuke Namekata, Kiyoshi Ichimoto, Takako T. Ishii, and Kazunari Shibata. Sun-as-a-star Analysis of H α Spectra of a Solar Flare Observed by SMART/SDDI: Time Evolution of Red Asymmetry and Line Broadening. *ApJ*, 933(2):209, July 2022. doi: 10.3847/1538-4357/ac75cd.
- Mayank Narang, Manoj Puravankara, H. K. Vedantham, C. H. Ishwara-Chandra, Ayanabha De, Himanshu Tyagi, Bihan Banerjee, Prasanta K. Nayak, Arun Surya, B. Shridharan, Vinod C. Pathak, and Mihir Tripathi. uGMRT Survey of EXoplanets Around M-dwarfs (GS-EXAM): Radio Observations of GJ 1151. *AJ*, 168(6):265, December 2024. doi: 10.3847/1538-3881/ad84e4.
- Elisabeth R. Newton, Jonathan Irwin, David Charbonneau, Perry Berlind, Michael L. Calkins, and Jessica Mink. The H α Emission of Nearby M Dwarfs and its Relation to Stellar Rotation. *ApJ*, 834(1):85, January 2017. doi: 10.3847/1538-4357/834/1/85.
- Yuta Notsu, Takuya Shibayama, Hiroyuki Maehara, Shota Notsu, Takashi Nagao, Satoshi Honda, Takako T. Ishii, Daisaku Nogami, and Kazunari Shibata. Superflares on Solar-type Stars Observed with Kepler II. Photometric Variability of Superflare-generating Stars: A Signature of Stellar Rotation and Starspots. *ApJ*, 771(2):127, July 2013. doi: 10.1088/0004-637X/771/2/127.
- R. W. Noyes, L. W. Hartmann, S. L. Baliunas, D. K. Duncan, and A. H. Vaughan. Rotation, convection, and magnetic activity in lower main-sequence stars. *ApJ*, 279:763–777, April 1984. doi: 10.1086/161945.
- Philip A. Nutzman, Daniel C. Fabrycky, and Jonathan J. Fortney. Using Star Spots to Measure the Spin-orbit Alignment of Transiting Planets. *ApJ*, 740(1):L10, October 2011. doi: 10.1088/2041-8205/740/1/L10.

- Antonija Oklopčić. Helium Absorption at 1083 nm from Extended Exoplanet Atmospheres: Dependence on Stellar Radiation. *ApJ*, 881(2):133, August 2019. doi: 10.3847/1538-4357/ab2f7f.
- Antonija Oklopčić and Christopher M. Hirata. A New Window into Escaping Exoplanet Atmospheres: 10830 Å Line of Helium. *ApJ*, 855(1):L11, March 2018. doi: 10.3847/2041-8213/aaada9.
- M. Oshagh, N. C. Santos, I. Boisse, G. Boué, M. Montalto, X. Dumusque, and N. Haghighipour. Effect of stellar spots on high-precision transit light-curve. *A&A*, 556:A19, August 2013. doi: 10.1051/0004-6361/201321309.
- Isabella Pagano, Antonino F. Lanza, Giuseppe Leto, Sergio Messina, Pierre Barge, and Annie Baglin. CoRoT-2a Magnetic Activity: Hints for Possible Star–Planet Interaction. *Earth Moon and Planets*, 105(2-4):373–378, September 2009. doi: 10.1007/s11038-009-9301-3.
- Luis Peña-Moñino and Miguel Pérez-Torres. Modelling magnetic star-planet interaction in the iconic M dwarfs Proxima Centauri, YZ Ceti and GJ 1151. *MNRAS*, September 2025. doi: 10.1093/mnras/staf1467.
- F. Pepe, M. Mayor, F. Galland, D. Naef, D. Queloz, N. C. Santos, S. Udry, and M. Burnet. The CORALIE survey for southern extra-solar planets VII. Two short-period Saturnian companions to <ASTROBJ>HD 108147</ASTROBJ> and <ASTROBJ>HD 168746</ASTROBJ>. *A&A*, 388: 632–638, June 2002. doi: 10.1051/0004-6361:20020433.
- M. Pérez-Torres, J. F. Gómez, J. L. Ortiz, P. Leto, G. Anglada, J. L. Gómez, E. Rodríguez, C. Triguero, P. J. Amado, A. Alberdi, G. Anglada-Escudé, M. Osorio, G. Umama, Z. Berdiñas, M. J. López-González, N. Morales, C. Rodríguez-López, and J. Chibueze. Monitoring the radio emission of Proxima Centauri. *A&A*, 645:A77, January 2021. doi: 10.1051/0004-6361/202039052.
- Luis Peña-Moñino and Miguel Pérez-Torres. Modelling magnetic star–planet interaction in the iconic m dwarfs proxima centauri, yz ceti, and gj 1151. *Monthly Notices of the Royal Astronomical Society*, 544(1):1220–1237, 11 2025. ISSN 0035-8711. doi: 10.1093/mnras/staf1467. URL <https://doi.org/10.1093/mnras/staf1467>.
- J. Sebastian Pineda and Jackie Villadsen. Coherent radio bursts from known M-dwarf planet-host YZ Ceti. *Nature Astronomy*, 7:569–578, May 2023. doi: 10.1038/s41550-023-01914-0.
- D. Queloz, G. W. Henry, J. P. Sivan, S. L. Baliunas, J. L. Beuzit, R. A. Donahue, M. Mayor, D. Naef, C. Perrier, and S. Udry. No planet for HD 166435. *A&A*, 379:279–287, November 2001. doi: 10.1051/0004-6361:20011308.
- Benjamin V. Rackham, Dániel Apai, and Mark S. Giampapa. The Transit Light Source Effect: False Spectral Features and Incorrect Densities for M-dwarf Transiting Planets. *ApJ*, 853(2):122, February 2018. doi: 10.3847/1538-4357/aaa08c.
- D. Revilla, P. J. Amado, R. Luque, P. Schöfer, A. Binnenfeld, J. A. Caballero, A. P. Hatzes, G. W. Henry, S. Jeffers, S. Kaur, A. F. Lanza, E. Pallé, L. Peña-Moñino, M. Pérez-Torres, A. Quirrenbach, A. Reiners, I. Ribas, D. Viganò, and S. Zucker. Planet-induced periodic modulation of stellar activity in GJ 436: Insights into a warm Neptune’s magnetic field. *A&A*, 2026. doi: 10.48550/arXiv.2604.06969. arXiv:2604.06969.
- D. Revilla, P. J. Amado, R. Luque, P. Schöfer, A. Binnenfeld, J. A. Caballero, Artie P. Hatzes, G. W. Henry, S. Jeffers, S. Kaur, A. F. Lanza, E. Pallé, L. Peña-Moñino, M. Pérez-Torres, A. Quirrenbach, A. Reiners, I. Ribas, D. Viganò, and S. Zucker. Planet-induced Periodic Modulation of Stellar Activity in GJ~436: Insights into a Warm Neptune’s Magnetic Field. *arXiv e-prints*, art. arXiv:2604.06969, April 2026. doi: 10.48550/arXiv.2604.06969.
- Agustín Sánchez-Lavega, Patrick Irwin, and Antonio García Muñoz. Dynamics and clouds in planetary atmospheres from telescopic observations. *A&A Rev.*, 31(1):5, December 2023. doi: 10.1007/s00159-023-00150-9.

- Roberto Sanchis-Ojeda and Joshua N. Winn. Starspots, Spin-Orbit Misalignment, and Active Latitudes in the HAT-P-11 Exoplanetary System. *ApJ*, 743(1):61, December 2011. doi: 10.1088/0004-637X/743/1/61.
- J. Sanz-Forcada and A. K. Dupree. Active cool stars and He I 10 830 Å: the coronal connection. *A&A*, 488(2):715–721, September 2008. doi: 10.1051/0004-6361:20078501.
- Joachim Saur, Thomas Grambusch, Stefan Duling, Fritz M. Neubauer, and Sven Simon. Magnetic energy fluxes in sub-alfvénic star–planet interactions. *Astronomy & Astrophysics*, 552:A119, 2013. doi: 10.1051/0004-6361/201118179.
- A. Savitzky and M. J. E. Golay. Smoothing and differentiation of data by simplified least squares procedures. *Analytical Chemistry*, 36:1627–1639, January 1964. doi: 10.1021/ac60214a047.
- J. D. Scargle. Studies in astronomical time series analysis. II. Statistical aspects of spectral analysis of unevenly spaced data. *ApJ*, 263:835–853, December 1982. doi: 10.1086/160554.
- Patrick Schöfer. *Activity of M dwarfs in the CARMENES sample*. Phd thesis, Institut für Astrophysik, Göttingen, Germany, 2021. Available at DOI:10.53846/goediss-8951.
- Ethan Schreyer, James E. Owen, Jessica J. Spake, Zahra Bahroloom, and Simone Di Giampasquale. Using helium 10 830 Å transits to constrain planetary magnetic fields. *MNRAS*, 527(3):5117–5130, January 2024. doi: 10.1093/mnras/stad3528.
- I. F. Shaikhislamov, L. Fossati, M. L. Khodachenko, H. Lammer, A. García Muñoz, A. Youngblood, N. K. Dwivedi, and M. S. Rumenskikh. Three-dimensional hydrodynamic simulations of the upper atmosphere of π Men c: Comparison with Ly α transit observations. *A&A*, 639:A109, July 2020. doi: 10.1051/0004-6361/202038363.
- E. Shkolnik, G. A. H. Walker, and D. A. Bohlender. Evidence for Planet-induced Chromospheric Activity on HD 179949. *ApJ*, 597(2):1092–1096, November 2003. doi: 10.1086/378583.
- E. Shkolnik, G. A. H. Walker, and D. A. Bohlender. Evidence for planet-induced chromospheric activity on hd 179949. *ApJ*, 597(2):1092, nov 2003. doi: 10.1086/378583.
- E. Shkolnik, G. A. H. Walker, D. A. Bohlender, P.-G. Gu, and M. Kürster. Hot Jupiters and Hot Spots: The Short- and Long-Term Chromospheric Activity on Stars with Giant Planets. *ApJ*, 622(2):1075–1090, April 2005. doi: 10.1086/428037.
- E. Shkolnik, G. A. H. Walker, D. A. Bohlender, P.-G. Gu, and M. Kurster. Hot jupiters and hot spots: The short- and long-term chromospheric activity on stars with giant planets. *ApJ*, 622(2):1075–1090, 2005. doi: 10.1086/428037.
- Evgenya Shkolnik, David A. Bohlender, Gordon A. H. Walker, and Andrew Collier Cameron. The On/Off Nature of Star-Planet Interactions. *ApJ*, 676(1):628–638, March 2008a. doi: 10.1086/527351.
- Evgenya Shkolnik, David A. Bohlender, Gordon A. H. Walker, and Andrew Collier Cameron. The On/Off Nature of Star-Planet Interactions. *ApJ*, 676(1):628–638, March 2008b. doi: 10.1086/527351.
- A. M. Silva, J. P. Faria, N. C. Santos, S. G. Sousa, P. T. P. Viana, J. H. C. Martins, P. Figueira, C. Lovis, F. Pepe, S. Cristiani, R. Rebolo, R. Allart, A. Cabral, A. Mehner, A. Sozzetti, A. Suárez Mascareño, C. J. A. P. Martins, D. Ehrenreich, D. Mégevand, E. Palte, G. Lo Curto, H. M. Taberero, J. Lillo-Box, J. I. González Hernández, M. R. Zapatero Osorio, N. C. Hara, N. J. Nunes, P. Di Marcantonio, S. Udry, V. Adibekyan, and X. Dumusque. A novel framework for semi-Bayesian radial velocities through template matching. *A&A*, 663:A143, July 2022. doi: 10.1051/0004-6361/202142262.
- A. M. Silva, N. C. Santos, J. P. Faria, J. H. C. Martins, E. A. S. Cristo, S. G. Sousa, P. T. P. Viana, É. Artigau, K. Al Moulla, A. Castro-González, D. F. M. Folha, P. Figueira, T. Schmidt, F. Pepe, X. Dumusque, O. D. S. Demangeon, T. L. Campante, X. Delfosse, B. Wehbe, J. Lillo-Box, A. R. Costa Silva, J. Rodrigues, J. I. González Hernández, T. Azevedo Silva, S. Cristiani, H. M. Taberero, E. Palte, B. Lavie, A. Suárez Mascareño, P. Di Marcantonio, A. Cabral, C. J. A. P. Martins, N. J. Nunes, and A. Sozzetti. A systematic bias in template-based radial velocity extraction algorithms. *A&A*, 700:A93, August 2025. doi: 10.1051/0004-6361/202554955.

- Adriana V. R. Silva. Method for Spot Detection on Solar-like Stars. *ApJ*, 585(2):L147–L150, March 2003. doi: 10.1086/374324.
- A. Silva-Valio and A. F. Lanza. Time evolution and rotation of starspots on CoRoT-2 from the modelling of transit photometry. *A&A*, 529:A36, May 2011. doi: 10.1051/0004-6361/201015382.
- U. Simola, X. Dumusque, and J. Cisewski-Kehe. Measuring precise radial velocities and cross-correlation function line-profile variations using a Skew Normal density. *A&A*, 622:A131, February 2019. doi: 10.1051/0004-6361/201833895.
- Jeffrey C. Smith, Martin C. Stumpe, Jeffrey E. Van Cleve, Jon M. Jenkins, Thomas S. Barclay, Michael N. Fanelli, Forrest R. Girouard, Jeffery J. Kolodziejczak, Sean D. McCauliff, Robert L. Morris, and Joseph D. Twicken. Kepler Presearch Data Conditioning II - A Bayesian Approach to Systematic Error Correction. *PASP*, 124(919):1000, September 2012. doi: 10.1086/667697.
- A. Strugarek, E. Bolmont, S. Mathis, A. S. Brun, V. Réville, F. Gallet, and C. Charbonnel. The Fate of Close-in Planets: Tidal or Magnetic Migration? *ApJ*, 847(2):L16, October 2017. doi: 10.3847/2041-8213/aa8d70.
- Martin C. Stumpe, Jeffrey C. Smith, Jeffrey E. Van Cleve, Joseph D. Twicken, Thomas S. Barclay, Michael N. Fanelli, Forrest R. Girouard, Jon M. Jenkins, Jeffery J. Kolodziejczak, Sean D. McCauliff, and Robert L. Morris. Kepler Presearch Data Conditioning I—Architecture and Algorithms for Error Correction in Kepler Light Curves. *PASP*, 124(919):985, September 2012. doi: 10.1086/667698.
- Martin C. Stumpe, Jeffrey C. Smith, Joseph H. Catanzarite, Jeffrey E. Van Cleve, Jon M. Jenkins, Joseph D. Twicken, and Forrest R. Girouard. Multiscale Systematic Error Correction via Wavelet-Based Bandsplitting in Kepler Data. *PASP*, 126(935):100, January 2014. doi: 10.1086/674989.
- A. Suárez Mascareño, R. Rebolo, J. I. González Hernández, and M. Esposito. Rotation periods of late-type dwarf stars from time series high-resolution spectroscopy of chromospheric indicators. *MNRAS*, 452(3):2745–2756, September 2015. doi: 10.1093/mnras/stv1441.
- V. Y. D. Sumida, R. Estrela, M. Swain, and A. Valio. Where does the simplified stellar contamination model fail in exoplanet transmission spectroscopy? *A&A*, 706:A281, February 2026. doi: 10.1051/0004-6361/202556358.
- Jamila S. Taaki, Farzad Kamalabadi, and Athol J. Kemball. Bayesian Methods for Joint Exoplanet Transit Detection and Systematic Noise Characterization. *AJ*, 159(6):283, June 2020. doi: 10.3847/1538-3881/ab8e38.
- Giovanna Tinetti, Pierre Drossart, Paul Eccleston, Paul Hartogh, Astrid Heske, Jérémy Leconte, Giusi Micela, Marc Ollivier, Göran Pilbratt, Ludovic Puig, Diego Turrini, Bart Vandenbussche, Paulina Wolkenberg, Jean-Philippe Beaulieu, Lars A. Buchave, Martin Ferus, Matt Griffin, Manuel Guedel, Kay Justtanont, Pierre-Olivier Lagage, Pedro Machado, Giuseppe Malaguti, Michiel Min, Hans Ulrik Nørgaard-Nielsen, Mirek Rataj, Tom Ray, Ignasi Ribas, Mark Swain, Robert Szabo, Stephanie Werner, Joanna Barstow, Matt Burleigh, James Cho, Vincent Coudé du Foresto, Athena Coustenis, Leen Decin, Therese Encrenaz, Marina Galand, Michael Gillon, Ravit Helled, Juan Carlos Morales, Antonio García Muñoz, Andrea Moneti, Isabella Pagano, Enzo Pascale, Giuseppe Piccioni, David Pinfield, Subhajit Sarkar, Franck Selsis, Jonathan Tennyson, Amaury Triaud, Olivia Venot, Ingo Waldmann, David Waltham, Gillian Wright, Jerome Amiaux, Jean-Louis Auguères, Michel Berthé, Naidu Bezawada, Georgia Bishop, Neil Bowles, Deirdre Coffey, Josep Colomé, Martin Crook, Pierre-Elie Crouzet, Vania Da Peppo, Isabel Escudero Sanz, Mauro Focardi, Martin Frericks, Tom Hunt, Ralf Kohley, Kevin Middleton, Gianluca Morgante, Roland Ottensamer, Emanuele Pace, Chris Pearson, Richard Stamper, Kate Symonds, Miriam Rengel, Etienne Renotte, Peter Ade, Laura Affer, Christophe Alard, Nicole Allard, Francesca Altieri, Yves André, Claudio Arena, Ioannis Argyriou, Alan Aylward, Cristian Baccani, Gaspar Bakos, Marek Banaszekiewicz, Mike Barlow, Virginie Batista, Giancarlo Bellucci, Serena Benatti, Pernelle Bernardi, Bruno Bézard, Maria Blecka, Emeline Bolmont, Bertrand Bonfond, Rosaria Bonito, Aldo S. Bonomo, John Robert Brucato, Allan Sacha Brun, Ian Bryson, Waldemar Bujwan, Sarah Casewell, Benjamin Charnay, Cesare Cecchi Pestellini, Guo Chen, Angela Ciaravella, Riccardo Claudi, Rodolphe Clédassou, Mario

- Damasso, Mario Damiano, Camilla Danielski, Pieter Deroo, Anna Maria Di Giorgio, Carsten Dominik, Vanessa Doublier, Simon Doyle, René Doyon, Benjamin Drummond, Bastien Duong, Stephen Eales, Billy Edwards, Maria Farina, Ettore Flaccomio, Leigh Fletcher, François Forget, Steve Fossey, Markus Fränz, Yuka Fujii, Álvaro García-Piquer, Walter Gear, Hervé Geoffroy, Jean Claude Gérard, Lluís Gesa, H. Gomez, Rafał Graczyk, Caitlin Griffith, Denis Grodent, Mario Giuseppe Guarcello, Jacques Gustin, Keiko Hamano, Peter Hargrave, Yann Hello, Kevin Heng, Enrique Herrero, Allan Hornstrup, Benoit Hubert, Shigeru Ida, Masahiro Ikoma, Nicolas Iro, Patrick Irwin, Christopher Jarchow, Jean Jaubert, Hugh Jones, Queyrel Julien, Shingo Kameda, Franz Kerschbaum, Pierre Kervella, Tommi Koskinen, Matthijs Krijger, Norbert Krupp, Marina Lafarga, Federico Landini, Emanuel Lellouch, Giuseppe Leto, A. Luntzer, Theresa Rank-Lüftinger, Antonio Maggio, Jesus Maldonado, Jean-Pierre Maillard, Urs Mall, Jean-Baptiste Marquette, Stéphane Mathis, Pierre Maxted, Taro Matsuo, Alexander Medvedev, Yamila Miguel, Vincent Minier, Giuseppe Morello, Alessandro Mura, Norio Narita, Valerio Nascimbeni, N. Nguyen Tong, Vladimiro Noce, Fabrizio Oliva, Enric Palle, Paul Palmer, Maurizio Pancrazzi, Andreas Papageorgiou, Vivien Parmentier, Manuel Perger, Antonino Petralia, Stefano Pezzuto, Ray Pierrehumbert, and Ignazio Pillitteri. A chemical survey of exoplanets with ARIEL. *Experimental Astronomy*, 46(1):135–209, November 2018. doi: 10.1007/s10686-018-9598-x.
- Benjamin M. Tofflemire, Robert D. Mathieu, David R. Ardila, Rachel L. Akeson, David R. Ciardi, Christopher Johns-Krull, Gregory J. Herczeg, and Alberto Quijano-Vodniza. Accretion and Magnetic Reconnection in the Classical T Tauri Binary DQ Tau. *ApJ*, 835(1):8, January 2017. doi: 10.3847/1538-4357/835/1/8.
- T. Trifonov, M. Kürster, M. Zechmeister, L. Tal-Or, J. A. Caballero, A. Quirrenbach, P. J. Amado, I. Ribas, A. Reiners, S. Reffert, S. Dreizler, A. P. Hatzes, A. Kaminski, R. Launhardt, Th. Henning, D. Montes, V. J. S. Béjar, R. Mundt, A. Pavlov, J. H. M. M. Schmitt, W. Seifert, J. C. Morales, G. Nowak, S. V. Jeffers, C. Rodríguez-López, C. del Burgo, G. Anglada-Escudé, J. López-Santiago, R. J. Mathar, M. Ammler-von Eiff, E. W. Guenther, D. Barrado, J. I. González Hernández, L. Mancini, J. Stürmer, M. Abril, J. Aceituno, F. J. Alonso-Floriano, R. Antona, H. Anwand-Heerwart, B. Arroyo-Torres, M. Azzaro, D. Baroch, F. F. Bauer, S. Becerril, D. Benítez, Z. M. Berdiñas, G. Bergond, M. Blümcke, M. Brinkmüller, J. Cano, M. C. Cárdenas Vázquez, E. Casal, C. Cifuentes, A. Claret, J. Colomé, M. Cortés-Contreras, S. Czesla, E. Díez-Alonso, C. Feiz, M. Fernández, I. M. Ferro, B. Fuhrmeister, D. Galadí-Enríquez, A. García-Piquer, M. L. García Vargas, L. Gesa, V. Gómez Galera, R. González-Peinado, U. Grözing, S. Grohnert, J. Guàrdia, A. Guijarro, E. de Guindos, J. Gutiérrez-Soto, H.-J. Hagen, P. H. Hauschildt, R. P. Hedrosa, J. Helmling, I. Hermelo, R. Hernández Arabí, L. Hernández Castaño, F. Hernández Hernando, E. Herrero, A. Huber, P. Huke, E. Johnson, E. de Juan, M. Kim, R. Klein, J. Klüter, A. Klutsch, M. Lafarga, M. Lampón, L. M. Lara, W. Laun, U. Lemke, R. Lenzen, M. López del Fresno, M. J. López-González, M. López-Puertas, J. F. López Salas, R. Luque, H. Magán Madinabeitia, U. Mall, H. Mandel, E. Marfil, J. A. Marín Molina, D. Maroto Fernández, E. L. Martín, S. Martín-Ruiz, C. J. Marvin, E. Mirabet, A. Moya, M. E. Moreno-Raya, E. Nagel, V. Naranjo, L. Nortmann, A. Ofir, R. Oreiro, E. Pallé, J. Panduro, J. Pascual, V. M. Passegger, S. Pedraz, A. Pérez-Calpena, D. Pérez Medialdea, M. Perger, M. A. C. Perryman, M. Pluto, O. Rabaza, A. Ramón, R. Rebolo, P. Redondo, S. Reinhardt, P. Rhode, H.-W. Rix, F. Rodler, E. Rodríguez, A. Rodríguez Trinidad, R.-R. Rohloff, A. Rosich, S. Sadegi, E. Sánchez-Blanco, M. A. Sánchez Carrasco, A. Sánchez-López, J. Sanz-Forcada, P. Sarkis, L. F. Sarmiento, S. Schäfer, J. Schiller, P. Schöfer, A. Schweitzer, E. Solano, O. Stahl, J. B. P. Strachan, J. C. Suárez, H. M. Tabernero, M. Tala, S. M. Tulloch, G. Veredas, J. I. Vico Linares, F. Vilardell, K. Wagner, J. Winkler, V. Wolthoff, W. Xu, F. Yan, and M. R. Zapatero Osorio. The CARMENES search for exoplanets around M dwarfs . First visual-channel radial-velocity measurements and orbital parameter updates of seven M-dwarf planetary systems. *A&A*, 609:A117, February 2018. doi: 10.1051/0004-6361/201731442.
- Corrado Triglio, Ayan Biswas, Paolo Leto, Grazia Umama, Innocenza Busa, Francesco Cavallaro, Barnali Das, Poonam Chandra, Miguel Perez-Torres, Gregg A. Wade, Cristobal Bordiu, Carla S. Buemi, Filomena Bufano, Adriano Ingallinera, Sara Loru, and Simone Riggi. Star-Planet Interaction at radio wavelengths in YZ Ceti: Inferring planetary magnetic field. *arXiv e-prints*, art. arXiv:2305.00809, May 2023. doi: 10.48550/arXiv.2305.00809.

- Jake D. Turner, Philippe Zarka, Jean-Mathias Grießmeier, Joseph Lazio, Baptiste Cecconi, J. Emilio Enriquez, Julien N. Girard, Ray Jayawardhana, Laurent Lamy, Jonathan D. Nichols, and Imke de Pater. The search for radio emission from the exoplanetary systems 55 Cancri, ν Andromedae, and τ Boötis using LOFAR beam-formed observations. *A&A*, 645:A59, January 2021. doi: 10.1051/0004-6361/201937201.
- Stephen Turnpenney, Jonathan D. Nichols, Graham A. Wynn, and Sarah L. Casewell. Exoplanetary radio emission under realistic stellar wind conditions. *Monthly Notices of the Royal Astronomical Society*, 475(4):5644–5661, 2018. doi: 10.1093/mnras/sty143.
- Adriana Valio, Raissa Estrela, Yuri Netto, J. P. Bravo, and J. R. de Medeiros. Activity and Rotation of Kepler-17. *ApJ*, 835(2):294, February 2017. doi: 10.3847/1538-4357/835/2/294.
- Adriana Valio, Alexandre Araújo, and Fabian Menezes. Differential Rotation of CoRoT Stars and a Kepler Binary Star from Starspot Transit Mapping. *ApJ*, 972(1):81, September 2024. doi: 10.3847/1538-4357/ad66cb.
- H. K. Vedantham, J. R. Callingham, T. W. Shimwell, C. Tasse, B. J. S. Pope, M. Bedell, I. Snellen, P. Best, M. J. Hardcastle, M. Haverkorn, A. Mechev, S. P. O’Sullivan, H. J. A. Röttgering, and G. J. White. Coherent radio emission from a quiescent red dwarf indicative of star-planet interaction. *Nature Astronomy*, 4:577–583, February 2020. doi: 10.1038/s41550-020-1011-9.
- Krisztián Vida and Rachael M. Roettenbacher. Finding flares in Kepler data using machine-learning tools. *A&A*, 616:A163, September 2018. doi: 10.1051/0004-6361/201833194.
- A. Vidal-Madjar, A. Lecavelier des Etangs, J.-M. Désert, G. E. Ballester, R. Ferlet, G. Hébrard, and M. Mayor. An extended upper atmosphere around the extrasolar planet HD209458b. *Nature*, 422(6928):143–146, March 2003. doi: 10.1038/nature01448.
- A. Vidal-Madjar, J.-M. Désert, A. Lecavelier des Etangs, G. Hébrard, G. E. Ballester, D. Ehrenreich, R. Ferlet, J. C. McConnell, M. Mayor, and C. D. Parkinson. Detection of Oxygen and Carbon in the Hydrodynamically Escaping Atmosphere of the Extrasolar Planet HD 209458b. *ApJ*, 604(1):L69–L72, March 2004. doi: 10.1086/383347.
- Carolina Villarreal D’Angelo, Aline A. Vidotto, Alejandro Esquivel, Gopal Hazra, and Allison Youngblood. GJ 436b and the stellar wind interaction: simulations constraints using Ly α and H α transits. *MNRAS*, 501(3):4383–4395, March 2021. doi: 10.1093/mnras/staa3867.
- B. Y. Welsh, R. Lallement, J.-L. Vergely, and S. Raimond. New 3D gas density maps of NaI and CaII interstellar absorption within 300 pc. *A&A*, 510:A54, February 2010. doi: 10.1051/0004-6361/200913202.
- David J. Wilson, Cynthia S. Froning, Girish M. Duvvuri, Allison Youngblood, Kevin France, Alexander Brown, P. Christian Schneider, Zachory Berta-Thompson, Andrea P. Buccino, Jeffrey Linsky, R. O. Parke Loyd, Yamila Miguel, Elisabeth Newton, J. Sebastian Pineda, Seth Redfield, Aki Roberge, Sarah Rugheimer, and Mariela C. Vieytes. The Mega-MUSCLES Treasury Survey: X-Ray to Infrared Spectral Energy Distributions of a Representative Sample of M Dwarfs. *ApJ*, 978(1):85, January 2025. doi: 10.3847/1538-4357/ad9251.
- O. C. Wilson. Chromospheric variations in main-sequence stars. *ApJ*, 226:379–396, December 1978. doi: 10.1086/156618.
- A. Wyttenbach, P. Mollière, D. Ehrenreich, H. M. Cegla, V. Bourrier, C. Lovis, L. Pino, R. Allart, J. V. Seidel, H. J. Hoeijmakers, L. D. Nielsen, B. Lavie, F. Pepe, X. Bonfils, and I. A. G. Snellen. Mass-loss rate and local thermodynamic state of the KELT-9 b thermosphere from the hydrogen Balmer series. *A&A*, 638:A87, June 2020. doi: 10.1051/0004-6361/201937316.
- Dongdong Yan, Jianheng Guo, Chenliang Huang, and Lei Xing. Atmosphere Escape Inferred from Modeling the H α Transmission Spectrum of WASP-121b. *ApJ*, 907(2):L47, February 2021. doi: 10.3847/2041-8213/abda41.

- Fei Yan and Thomas Henning. An extended hydrogen envelope of the extremely hot giant exoplanet KELT-9b. *Nature Astronomy*, 2:714–718, July 2018. doi: 10.1038/s41550-018-0503-3.
- Samuel W. Yee, Joshua N. Winn, Heather A. Knutson, Kishore C. Patra, Shreyas Vissapragada, Michael M. Zhang, Matthew J. Holman, Avi Shporer, and Jason T. Wright. The Orbit of WASP-12b Is Decaying. *ApJ*, 888(1):L5, January 2020. doi: 10.3847/2041-8213/ab5c16.
- Roger V. Yelle. Corrigendum to “Aeronomy of extra-solar giant planets at small orbital distances” [Icarus 170 (2004) 167–179]. *Icarus*, 183(2):508–508, August 2006. doi: 10.1016/j.icarus.2006.05.001.
- Allison Youngblood, Kevin France, R. O. Parke Loyd, Jeffrey L. Linsky, Seth Redfield, P. Christian Schneider, Brian E. Wood, Alexander Brown, Cynthia Froning, Yamila Miguel, Sarah Rugheimer, and Lucianne Walkowicz. The MUSCLES Treasury Survey. II. Intrinsic $LY\alpha$ and Extreme Ultraviolet Spectra of K and M Dwarfs with Exoplanets*. *ApJ*, 824(2):101, June 2016. doi: 10.3847/0004-637X/824/2/101.
- S. M. Zaleski, A. Valio, B. D. Carter, and S. C. Marsden. Dynamo activity of the K dwarf KOI-883 from transit photometry mapping. *MNRAS*, 510(4):5348–5361, March 2022. doi: 10.1093/mnras/stab3788.
- Philippe Zarka. Plasma interactions of exoplanets with their parent star and associated radio emissions. *Space Science Reviews*, 133(1-4):369–381, 2007. doi: 10.1007/s11214-007-9154-2.
- Philippe Zarka. Auroral radio emissions at planets: what do we learn from the solar system? what do we expect from exoplanets? *The Astronomy and Astrophysics Review*, 26(1):2, 2018. doi: 10.1007/s00159-017-0109-5.
- M. Zechmeister and M. Kürster. The generalised Lomb-Scargle periodogram. A new formalism for the floating-mean and Keplerian periodograms. *A&A*, 496(2):577–584, March 2009. doi: 10.1051/0004-6361:200811296.
- M. Zechmeister, A. Reiners, P. J. Amado, M. Azzaro, F. F. Bauer, V. J. S. Béjar, J. A. Caballero, E. W. Guenther, H. J. Hagen, S. V. Jeffers, A. Kaminski, M. Kürster, R. Launhardt, D. Montes, J. C. Morales, A. Quirrenbach, S. Reffert, I. Ribas, W. Seifert, L. Tal-Or, and V. Wolthoff. Spectrum radial velocity analyser (SERVAL). High-precision radial velocities and two alternative spectral indicators. *A&A*, 609:A12, January 2018. doi: 10.1051/0004-6361/201731483.
- Zhoujian Zhang, Caroline V. Morley, Michael Gully-Santiago, Morgan MacLeod, Antonija Oklopčić, Jessica Luna, Quang H. Tran, Joe P. Ninan, Suvrath Mahadevan, Daniel M. Krolkowski, William D. Cochran, Brendan P. Bowler, Michael Endl, Gudmundur Stefánsson, Benjamin M. Tofflemire, Andrew Vanderburg, and Gregory R. Zeimann. Giant tidal tails of helium escaping the hot Jupiter HAT-P-32 b. *Science Advances*, 9(23):eadf8736, June 2023. doi: 10.1126/sciadv.adf8736.
- S. Zucker. Cross-correlation and maximum-likelihood analysis: a new approach to combining cross-correlation functions. *MNRAS*, 342(4):1291–1298, July 2003. doi: 10.1046/j.1365-8711.2003.06633.x.